International Journal of Biological Macromolecules 320 (2025) 145699

Contents lists available at ScienceDirect

International Journal of Biological Macromolecules

journal homepage: www.elsevier.com/locate/ijbiomac

Discovery of potential RAF selective back pocket as a promising biological site for BRAF inhibitors targeting resistant melanoma opens the door for a new generation of kinase inhibitors: Design, synthesis, biological evaluation, and *in silico* molecular simulation

Usama Ammar [a,*], Mahmoud Gamal El-Din [b], Mohammed Abdel-Maksoud [b], Eslam Ali [c], Mohammed I. El-Gamal [d,e], Zeyad Mahmoud [f,g], Sunjoo Ahn [h,i], Nhung Hong Nguyen [h,i], Eunkyoung Kim [h,i], Park Su Jun [j], Kim Young Deug [j], Hong Seok Choi [k], Kwan Hyi Lee [g,l], Gahyeon Choi [h,i], Chang-Hyun Oh [g,*]

[a] School of Applied Sciences, Edinburgh Napier University, Sighthill Campus, 9 Sighthill Court, Edinburgh EH11 4BN, United Kingdom
[b] Medicinal & Pharmaceutical Chemistry Department, Pharmaceutical and Drug Industries Research Division, National Research Centre (NRC), Dokki, Giza 12622, Egypt
[c] Drug Discovery Core, Comprehensive Cancer Center, University of Virginia, Charlottesville, VA 22904, USA
[d] Department of Medicinal Chemistry, College of Pharmacy and Research Institute for Medical and Health Sciences, University of Sharjah, Sharjah 27272, United Arab Emirates
[e] Department of Medicinal Chemistry, Faculty of Pharmacy, Mansoura University, Mansoura 35516, Egypt
[f] University of Science & Technology (UST), Daejeon, Yuseong-gu 34113, Republic of Korea
[g] Center for Biomaterials, Korea Institute of Science & Technology (KIST), 136-791 Seoul, Republic of Korea
[h] Therapeutics & Biotechnology Division, Korea Research Institute of Chemical Technology, Daejeon 34114, Republic of Korea
[i] Department of Medicinal Chemistry and Pharmacology, University of Science and Technology, Daejeon 34113, Republic of Korea
[j] CTCBIO Inc., Gyeonggi-do 18576, Republic of Korea
[k] College of Pharmacy, Chosun University, Gwangju 61452, Republic of Korea
[l] KU-KIST Graduate School of Converging Science and Technology, Korea University, Seoul 02841, Republic of Korea

ARTICLE INFO

Keywords:
BRAF kinase
Resistant melanoma
RAF back pocket
Drug design

ABSTRACT

Despite the approved combination of BRAF^{V600E} and MEK inhibitors to treat drug-resistant melanoma, serious side effects associated with this combination have been reported, particularly referring to MEK inhibitors. In the current study, an isosteric drug design strategy and were applied leading to the discovery of **KS16**, a highly potent candidate with a developed pharmacokinetic profile. **KS16** exhibited superior efficacy in inhibiting drug-resistant melanoma cell proliferation as a single agent. **KS16** displayed a selective cytotoxic profile against melanoma cell lines over other types of cancer cell lines and inhibited RAF kinases over other protein kinases. It showed potent *in vivo* activity against melanoma-bearing animal models. *In silico* molecular docking revealed potential hydrophobic interactions with RAF selective back pocket. **KS16** demonstrated improved microsomal stability, half-life, and bioavailability. It exhibited an improved safety profile over normal skin cell lines and hERG protein. Our ultimate future direction is to generate an advanced lead candidate.

1. Introduction

Risking the health of people worldwide, cancer pushed thousands of researchers to develop novel agents and therapeutic methods continuously despite the achievements made in medicinal chemistry [1,2]. Cancer is characterized by an upregulation in many complexes signalling pathways to accelerate tumor growth, proliferation, and mobility [3,4].

Because several kinases are involved in the growth of human cancers, protein kinases have emerged as a major class of targeted therapy [5–7].

* Corresponding authors.
E-mail addresses: u.ammar@napier.ac.uk (U. Ammar), choh@kist.re.kr (C.-H. Oh).

https://doi.org/10.1016/j.ijbiomac.2025.145699
Received 24 April 2025; Received in revised form 29 June 2025; Accepted 30 June 2025
Available online 7 July 2025

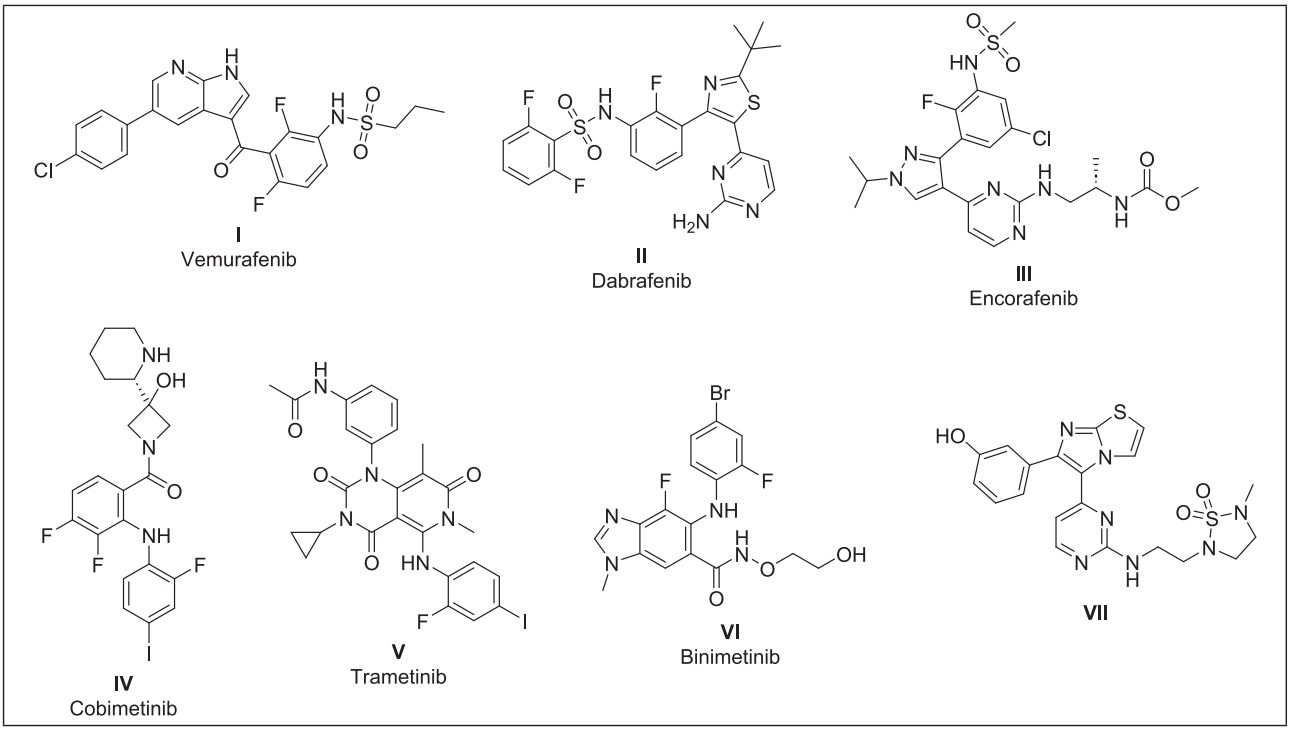

Fig. 1. Chemical structures of FDA approved drugs (**I-VI**) and our developed compound (**VII**) in the previous study.

Up to now, approximately 50 kinase inhibitors (KIs) have already been licensed by the US Food and Drug Administration (FDA), among them, 45 kinase inhibitors are currently being targeted for cancer treatment [5,8].

Uncontrolled protein kinase (PK) stimulation in response to mutations or overexpression is the main mechanism for cancer growth and propagation [9–11]. Hence PKs are considered crucial targets for the development of new, effective targeted cancer therapy [9,12,13].

In fundamental cellular functions, intracellular signal transduction occurs through the transfer of signal from cell surface to the nucleus resulting in cell division, differentiation, migration and apoptosis [9]. The process of signal transduction is controlled by a number of key cellular proteins such as receptor tyrosine kinases (RTKs), serine-threonine kinases (STKs), and G protein [9,11]. The high frequency of aberrant activity of the RAS/RAF/MEK/ERK cascade found in human cancers, makes this pathway a potential target for the treatment [14–17].

RAF family (the key component in MAPK signalling pathway) includes three members: ARAF, BRAF, and CRAF. Most of oncogenic mutations occur mostly in BRAF gene [18]. Oncogenic mutations in BRAF occur in around 50 % of melanoma patients but also in colon, adenocarcinoma (5–12 %), papillary thyroid carcinoma (39–69 %) and others. The point mutation in BRAF kinase enzyme is significantly contributed to the progression of melanoma skin cancer ($BRAF^{V600E}$). Where, it will be constitutively activated leading to uncontrolled cell proliferation (significantly associated with melanoma). The most common BRAF mutation, found in >90 % of BRAF-mutated tumors, is a substitution of a valine with a glutamic acid at amino acid 600 (V600E) in the kinase activation domain [18–22]. This substitution mimics phosphorylation of the activation loop, thereby inducing constitutive BRAF protein kinase activity that does not require external stimuli to be activated [22,23]. Consequently, the mutated BRAF phosphorylates and activates MEK kinase, which in turn phosphorylates and activates ERK kinase at Tyr 204/187 and Thr 202/185 residues [18].

FDA has approved vemurafenib **I** [18,24], dabrafenib **II** [18,25], and encorafenib **III** [26] (Fig. 1) as targeted therapies for the mutated BRAF ($BRAF^{V600E}$)-derived melanoma [24,25,27,28]. However, response to these single-targeted therapies is limited to 6–7 months of treatment due to the acquired drug resistance [18,25,29–33]. Mechanism of drug resistance is reported to pursue through activation of other key kinases in the same signalling pathway [34–40]. FDA has approved the combination targeted therapies between $BRAF^{V600E}$ inhibitors and MEK inhibitors, such as cobimetinib **IV**, trametinib **IV**, and binimetinib **VI** (Fig. 1), for the treatment of drug-resistant melanoma [41–44].

Unfortunately, serious side effects are associated with the approved combination therapies such as serious bleeding problems in stomach or brain that can lead to death, QT prolongation can cause irregular heartbeats that can be life-threatening, blood clots in arms or/and legs which can travel to lungs and can lead to death, muscle problems such as rhabdomyolysis, embro-fetal toxicity if administered to pregnant women [45–50]. Notably, the significant side effects associated with the combination targeted therapies are attributed to MEK inhibitors (cobimetinib **IV**, trametinib **IV**, and binimetinib **VI**) [42,51,52]. Drawing on the existing evidence, the drug discovery of new generation of small molecule candidate that inhibit MAPK signalling pathway, as a potential biological target in melanoma, may alter the disease course and avert the metastasis with minimal off-target effects and side effects. By delivering a new generation of BRAF inhibitors with potent pharmacological profile against drug-resistant melanoma, significant reduction in disease burden, associated with safety margins, will be achieved providing direct and indirect benefits across the global communities.

Previously, we have developed a potent series of imidazothiazole derivatives as pan RAF inhibitors that showed activity against melanoma cell line (**VII**, Fig. 1) [53]. In the current study, in term of drug development, we applied isosteric drug design strategy of our developed compounds to enhance the pharmacological activities across the melanoma cell lines (sensitive and resistant forms). The key rational design of our study is directing the RAF selective back pocket. The small sized gatekeeper (GK) amino acid residue (Thr 529) reveals a large sized and accessible back pocket with hydrophobic amino acid residues (Leu 505 – Val 528) which allow us incorporating hydrophobic and bulky group to anchor this unique region. Initially, we replaced the hinge binding motif into pyridine ring and the back pocket-directing group into different substituted phenyl ring (series A) to identify the potential binding mode.

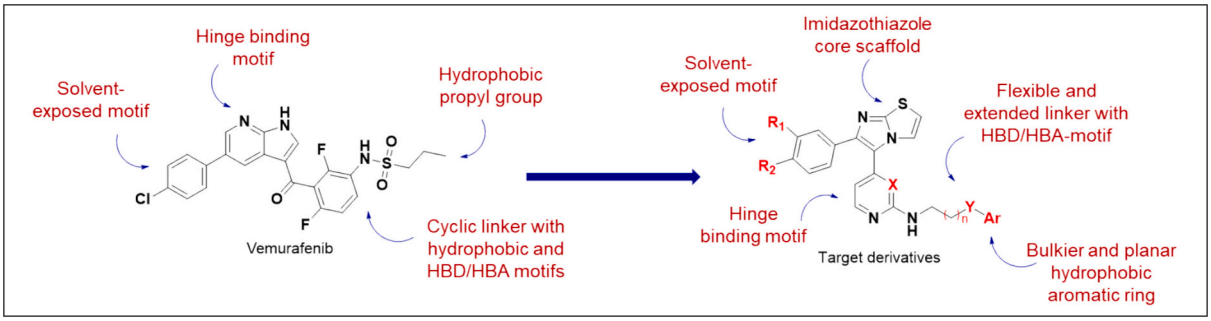

Fig. 2. The rational design of the developed compounds in this current study using vemurafenib **I** as lead compound. The bicyclic azaindole hinge binding motif was replaced with monocyclic 2-amino pyridine/pyrimidine. The cyclic linker (phenyl ring with sulphonamide group) between the terminal group and the hinge binding motif was replaced with extended open and flexible chain linker (two and three-carbon spacers). The terminal hydrophobic group (propyl group) was replaced with planar and hydrophobic aromatic ring (phenyl) decorated with different substituents with different size and chemical environment to accommodate the hydrophobic selective back pocket (Leu 505 – Val 528). The distal phenyl ring at the solvent-exposed area was decorated with HBD/HBA groups and additional F group, H-like atom, to investigate the possible new halogen binding interactions with the key amino acid residues at this area.

Additionally, we decorated the distal phenyl ring, solvent-exposed motif, with a small-sized fluorine atom (series B) to identify the possibility of halogen binding interaction with the key amino acid residues at the solvent-exposed area, along with the substituted aromatic ring at the RAF selective back pocket (Fig. 2).

We have investigated that the fluorinated derivatives (series B) showed potent profile against mutated BRAF kinase enzyme (nanomolar level) compared to that of vemurafenib **I**. One of the potent fluorinated compounds (22g; **KS16**) was selected among the potent series (series B) to be tested and evaluated to investigate its potential to inhibit the growth of both sensitive and resistant forms of melanoma cell lines using vemurafenib **I** as standard. Additionally, deep early drug discovery research activities were carried out to **KS16** such as expanded panel of biological and pharmacokinetic assays to develop a preclinical candidate in treating drug-resistant melanoma. Proudly, we have developed a small molecule inhibitor exhibited significant growth inhibition of a drug-resistant melanoma cell line, unlike vemurafenib **I**, which did not demonstrate the same inhibitory profile (resistant melanoma cell line viability = 25 % and 80 % at 10 μM, respectively). Our main target and future direction aim to generate an advanced lead candidate with enhanced pharmacokinetic profile (oral bioavailability and microsomal stability). Additionally, we will work actively with our collaborative groups to identify the possible mechanism of action of this candidate in particular within the resistant forms.

2. Materials and methods

2.1. Chemistry

2.1.1. General

All solvents and reagents were purchased from Merck, TCI Chemicals and DaeJung Chemicals and used without further purification. The key intermediates and final compounds and were purified by column chromatography using silica gel (0.040–0.063 mm, 230–400 mesh) and technical grade solvents. Analytical thin layer chromatography (TLC) was performed on silica gel 60 F254 plates from Merck. All spots were visualized at 365 nm and 254 nm by Spectroline UV ENF-240C/FE. All melting points were determined on Thomas-Hoover (Uni-Melt) Capillary Melting Point Apparatus. ^{1}H NMR and ^{13}C NMR spectra were recorded on Bruker Avance 400 and 500 spectrometers using TMS as an internal standard and signals are described as s (singlet), d (doublet), t (triplet), q (quartet), m (multiplet). LC-MS analysis was carried out using the following system: Waters 2998 photodiode array detector, Waters 3100 mass detector, Waters SFO system fluidics organizer, Waters 2545 binary gradient module, Waters reagent manager, Waters 2767 sample manager, Sunfire™ C18 column (4.6 × 50 mm, 5 μm particle size); Solvent gradient = 95 % A at 0 min, 1 % A at 5 min; solvent A: 0.035 % trifluoroacetic acid (TFA) in water; solvent B: 0.035 % TFA in MeOH; flow rate = 3.0 mL/min; the AUC was calculated using Waters MassLynx 4.1 software. Solvents and liquid reagents were transferred using hypodermic syringes. All compounds are >95 % pure by HPLC analysis (Figs. S55–142). All animal experiments were conducted in compliance with institutional guidelines.

2.1.2. Synthesis of methyl 3-methoxybenzoate (2)

Conc. sulfuric acid (2 mL) was added dropwise to a stirred solution of 3-methoxybenzoic acid (**1**, 20 g, 0.13 mol, 1 Eq) in MeOH (300 mL). The reaction mixture was allowed to stir under reflux for 18 h. The reaction mixture was allowed to cool and quenched with saturated solution of $NaHCO_3$ (50 mL). The reaction mixture was concentrated under reduced pressure. The produced ppt was filtered, washed with water (3 × 50 mL) and dried to give the titled product **2** (19 g, 88 %).

2.1.3. Synthesis of 2-(2-bromopyridin-4-yl)-1-(3-methoxyphenyl)Ethan-1-one (4)

Lithium bis(trimethylsilyl)amide solution (1.0 M in THF, 116 mL, 116.26 mmol, 2 Eq) was added dropwise to a solution of 2-bromo-4-methylpyridine (**3**, 10 g, 58.13 mmol, 1 Eq) in anhydrous THF (100 mL) at −78 °C. The reaction mixture was stirred for 30 min at −20 °C. A solution of methyl 3-methoxybenzoate (**2**, 9.7 g, 58.13 mmol, 1 Eq) in anhydrous THF (10 mL) was added dropwise to the previous mixture at −78 °C. The reaction mixture was allowed to stir at room temperature for 1 h. The reaction was quenched with saturated solution of NH_4Cl (100 mL). THF was removed under reduced pressure. The produced ppt was filtered, washed with MeOH (2 × 5 mL) and dried to give the titled product **4** as white crystals to be used in the next step without further purification (13 g).

2.1.4. Synthesis of 2-bromo-2-(2-bromopyridin-4-yl)-1-(3-methoxyphenyl) ethan-1-one (5)

A mixture of compound **4** (10 g, 32.66 mmol, 1 Eq) and *N*-bromosuccinimide (8.7 g, 49 mmol, 1.5 Eq) were dissolved in anhydrous DMF (50 mL). The reaction mixture was stirred at 60 °C for 3 h. The reaction mixture was cooled and extracted between EtOAc (70 mL) and water (200 mL). The organic layer was washed with brine (3 × 100 mL), dried over anhydrous Na_2SO_4 and evaporated under reduced pressure. The crude residue was triturated with MeOH. The produced solid was filtered and washed with MeOH and dried to give the titled produced **5** as white solid to be used in the next step without further purification (10 g).

2.1.5. Synthesis of 5-(2-bromopyridin-4-yl)-6-(3-methoxyphenyl)imidazo [2,1-b]thiazole (7)

A mixture of compound **5** (10 g, 26 mmol, 1 Eq) and thiazol-2-amine

Table 1
Key structure of series A (**11a-r** and **12a-r**).

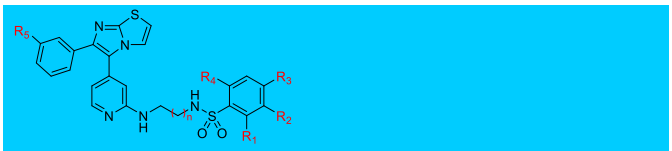

Compound	R_1	R_2	R_3	R_4	n	R_5
11a	H	H	H	H	1	OMe
11b	H	H	H	H	2	OMe
11c	H	H	CF_3	H	1	OMe
11d	H	H	CF_3	H	2	OMe
11e	H	H	OMe	H	1	OMe
11f	H	H	OMe	H	2	OMe
11 g	H	H	F	H	1	OMe
11 h	H	H	F	H	2	OMe
11i	H	H	Cl	H	1	OMe
11j	H	H	Cl	H	2	OMe
11 k	H	H	Br	H	1	OMe
11 l	H	H	Br	H	2	OMe
11 m	H	F	H	H	1	OMe
11n	H	F	H	H	2	OMe
11o	H	Cl	H	H	1	OMe
11p	H	Cl	H	H	2	OMe
11q	Cl	H	H	Cl	1	OMe
11r	Cl	H	H	Cl	2	OMe
12a	H	H	H	H	1	OH
12b	H	H	H	H	2	OH
12c	H	H	CF_3	H	1	OH
12d	H	H	CF_3	H	2	OH
12e	H	H	OH	H	1	OH
12f	H	H	OH	H	2	OH
12 g	H	H	F	H	1	OH
12 h	H	H	F	H	2	OH
12i	H	H	Cl	H	1	OH
12j	H	H	Cl	H	2	OH
12 k	H	H	Br	H	1	OH
12 l	H	H	Br	H	2	OH
12 m	H	F	H	H	1	OH
12n	H	F	H	H	2	OH
12o	H	Cl	H	H	1	OH
12p	H	Cl	H	H	2	OH
12q	Cl	H	H	Cl	1	OH
12r	Cl	H	H	Cl	2	OH

(**6**, 3.1 g, 31.2 mmol, 1.2 Eq) were dissolved in anhydrous acetonitrile. The reaction mixture was allowed to reflux for 18 h. The organic solvent was removed under vacuum. The crude residue was extracted between EtOAc (50 mL) and NH_4OH solution (50 mL). The organic layer was washed with brine (3 × 50 mL), dried over anhydrous Na_2SO_4 and evaporated under reduced pressure. The crude residue was purified through a thin layer of silica using 70 % EtOAc in hexane (200 mL) to give the titled product as white solid (5 g, 50 %).

*2.1.6. General procedure for synthesis of N^1-(4-(6-(3-methoxyphenyl) imidazo[2,1-b]thiazol-5-yl)pyridin-2-yl)ethane-1,2-(propane-1,3-)diamine (**9a,b**)*

A solution of compound **7** (5 g, 13 mmol, 1 Eq) in appropriate diamine (**8a,b**, 50 mL) was allowed to reflux for 30 h. The excess diamine was removed by distillation. The crude residue was extracted between EtOAc (20 mL) and NH_4OH solution (50 mL). The organic layer was washed with brine (3 × 50 mL), dried over anhydrous Na_2SO_4 and evaporated under reduced pressure to give the titled produced **9a,b** to be used in the next step without further purification.

*2.1.7. General procedure for synthesis of N-(2-((4-(6-(3-methoxyphenyl) imidazo[2,1-b]thiazol-5-yl)pyridin-2-yl)amino)ethyl(propyl)) arylsulfonamide (**11a-r**)*

A solution of appropriate arylsulfonyl chloride (**10a-j**, 1.65 mmol, 1.1 Eq) in anhydrous DCM (1 mL) was added dropwise to a solution of compound **9a,b** (1.5 mmol, 1 Eq) and triethylamine (0.46 g, 0.6 mL, 4.5 mmol, 3 Eq) in anhydrous DCM (2 mL) at 0 °C. The reaction mixture was allowed to stir at room temperature for 6 h. The reaction mixture was quenched with saturated solution of $NaHCO_3$ (2 mL). The organic layer was washed with brine (2 × 2 mL), dried over anhydrous Na_2SO_4 and evaporated under reduced pressure. The crude residue was purified using column chromatography (60 % EtOAc in hexane) to give the titled product **11a-r** (Table 1).

*2.1.8. General procedure for synthesis of N-(3-aminopropyl)unsubstituted and substituted phenyl sulfonamide (**13a-h**)*

A solution of appropriate aromatic sulfonyl chloride (**10a-h**, 5 mmol, 1 Eq) in dichloromethane (2 mL) was added dropwise to a solution of 1,3-diaminopropane (**8b**, 0.74 g, 0.8 mL, 10 mmol, 2 Eq) and trimethylamine (300 mg, 0.4 mL, 30 mmol, 6 Eq) in dichloromethane (20 mL) at 0 °C. The reaction mixture was allowed to stir at room temperature for 18 h. The reaction mixture was washed with saturated solution of $NaHCO_3$ (20 mL). The organic layer was dried over anhydrous Na_2SO_4 and evaporated under reduced pressure. The crude product was washed with hexane (2 × 10 mL) and dried to give the titled products **13a-h** to be used in the next steps without further purification [54].

*2.1.9. Synthesis of methyl 4-fluoro-3-methoxybenzoate (**15**)*

Sulfuric acid (1 mL) was added dropwise to a stirred solution of 4-fluoro-3-methoxybenzoic acid (**14**, 10 g, 58.78 mmol, 1 Eq) in MeOH (200 mL). The reaction mixture was allowed to stir under reflux for 18 h. The reaction mixture was allowed to cool and quenched with saturated solution of $NaHCO_3$ (50 mL). The reaction mixture was concentrated under reduced pressure. The produced ppt was filtered, washed with water (3 × 50 mL) and dried to give the titled product **14** (9 g, 83 %).

*2.1.10. Synthesis of 1-(4-fluoro-3-methoxyphenyl)-2-(2-(methylthio) pyrimidin-4-yl)ethan-1-one (**17**)*

Lithium bis(trimethylsilyl)amide solution (1.0 M in THF, 116 mL, 116.26 mmol, 2 Eq) was added dropwise to a solution of 4-methyl-2-(methylthio)pyrimidine (**16**, 8.2 g, 58.13 mmol, 1 Eq) in anhydrous THF (100 mL) at −78 °C. The reaction mixture was stirred for 30 min at −20 °C. A solution of methyl 4-fluoro-3-methoxybenzoate (**15**, 10.7 g, 58.13 mmol, 1 Eq) in anhydrous THF (10 mL) was added dropwise to the previous mixture at −78 °C. The reaction mixture was allowed to stir at room temperature for 1 h. The reaction was quenched with saturated solution of NH_4Cl (100 mL). THF was removed under reduced pressure. The produced ppt was filtered, washed with MeOH (2 × 5 mL) and dried to give the titled product **17** as yellow solid to be used in the next step without further purification (11 g).

*2.1.11. Synthesis of 2-bromo-1-(4-fluoro-3-methoxyphenyl)-2-(2-(methylthio)pyrimidin-4-yl)ethan-1-one (**18**)*

N-bromosuccinimide (9.1 g, 51.3 mmol, 1.5 Eq) was added to a solution of compound **17** (10 g, 34.21 mmol, 1 Eq) in anhydrous DCM (50 mL). The reaction mixture was stirred at room temperature for 30 min. The reaction mixture was quenched with water (100 mL). The organic layer was washed with brine (3 × 100 mL), dried over anhydrous Na_2SO_4 and evaporated under reduced pressure. The crude residue was triturated with MeOH. The produced solid was filtered and washed with MeOH and dried to give the titled produced **18** as white solid to be used in the next step without further purification (9 g).

2.1.12. Synthesis of 6-(4-fluoro-3-methoxyphenyl)-5-(2-(methylthio) pyrimidin-4-yl)imidazo[2,1-b]thiazole (19)

A mixture of compound **18** (9.65 g, 26 mmol, 1 Eq) and thiazol-2-amine (**6**, 3.1 g, 31.2 mmol, 1.2 Eq) were dissolved in anhydrous MeCN. The reaction mixture was allowed to reflux for 18 h. The organic solvent was removed under vacuum. The crude residue was purified through a thin layer of silica using 70 % EtOAc in hexane (200 mL) then triturated with MeOH to give the titled product **19** as white solid to be used in the next step without further purification (4 g).

2.1.13. Synthesis of 6-(4-fluoro-3-methoxyphenyl)-5-(2-(methylsulfonyl) pyrimidin-4-yl)imidazo[2,1-b]thiazole (20)

A solution of potassium peroxymonosulfate (25.7 g, 40.29 mmol, 3 Eq) in water (50 mL) was added to a solution of compound **19** (5 g, 13.43 mmol, 1 Eq) in MeOH (100 mL). The reaction mixture was stirred at room temperature for 48 h. The reaction mixture was concentrated under reduced pressure and washed with water (100 mL). The organic layer was washed with brine (2 × 50 mL), dried over anhydrous Na_2SO_4 and evaporated under reduced pressure. The crude residue was purified using column chromatography (60 % EtOAc in hexane) to give the titled product as white solid (3 g, 55 %).

2.1.14. General procedure for synthesis of N-substituted-4-(6-(4-fluoro-3-methoxyphenyl)imidazo[2,1-b]thiazol-5-yl)pyrimidin-2-amine (21a-h)

A mixture of compound **20** (0.5 g, 1.24 mmol, 1 Eq), appropriate amine (**13a-h**, 1.48 mmol, 1.2 Eq) and *N*,*N*-diisopropylethylamine (1.4 g, 2 mL, 11.16 mmol, 9 Eq) in anhydrous DMSO (2 mL). The reaction mixture was stirred at 90 °C for 9 h. The reaction mixture was cooled and extracted between EtOAc (10 mL) and water (30 mL). The organic layer was washed with water (3 × 30 mL). The organic layer was dried over anhydrous Na_2SO_4 and evaporated under reduced pressure. The crude residue was purified using column chromatography (50 % EtOAc in hexane) to give the titled product **21a-h** (Table 7).

2.1.15. General procedure for synthesis of N-substituted-4-(6-(4-fluoro-3-hydroxyphenyl)imidazo[2,1-b]thiazol-5-yl)pyrimidin-2-amine (22a-h)

Boron tribromide solution (1.0 M in DCM, 1 mL, 1 mmol, 5 Eq) was added dropwise to a solution of compound **21a-h** (0.2 mmol, 1 Eq) in anhydrous DCM (10 mL) at −10 °C. The reaction mixture was allowed to stir at room temperature for 6 h. The reaction mixture was quenched with saturated solution of $NaHCO_3$ (5 mL). The organic layer was washed with brine (2 × 5 mL), dried over anhydrous Na_2SO_4 and evaporated under reduced pressure. The crude residue was purified using column chromatography (80 % EtOAc in hexane) to give the titled product **22a-h** (Table 7).

2.2. In vitro NCI cytotoxicity screening

The synthesized compounds were tested and screened against a panel of 60 cancer cell lines (leukemia, non-small cell lung cancer, CNS cancer, melanoma, ovarian cancer, renal cancer, prostate cancer, and breast cancer cell lines) at the National Cancer Institute (NCI), Bethesda, Maryland, USA (www.dtp.nci.nih.gov) applying their standard protocol (https://dtp.cancer.gov/discovery_development/nci-60/methodology.htm). The synthesized compounds were initially tested at a single high dose (10 μM) in the full NCI 60 cell panel to identify the % growth inhibition (%GI). The compounds that exhibited significant growth inhibition were selected, based on the NCI historical DTP screening data, to be tested in 5-dose screening to explore the GI_{50} values.

The human tumor cell lines of the cancer screening panel were grown in RPMI 1640 medium containing 5 % fetal bovine serum and 2 mM L-glutamine. For a typical screening experiment, the cells were inoculated into 96 well microtiter plates in 100 μL at plating densities ranging from 5000 to 40,000 cells/well depending on the doubling time of individual cell lines. After cell inoculation, the microtiter plates were incubated at 37 °C, 5 % CO_2, 95 % air and 100 % relative humidity for 24 h prior to addition of experimental drugs.

After 24 h, two plates of each cell line were fixed *in situ* with TCA, to represent a measurement of the cell population for each cell line at the time of sample addition (Tz). The tested compounds were solubilized in dimethyl sulfoxide at 400-fold the desired final maximum test concentration and stored frozen prior to use. At the time of drug addition, an aliquot of frozen concentrate was thawed and diluted to twice the desired final maximum test concentration with complete medium containing 50 μg/mL gentamicin. Additional four, 10-fold or 1/2 log serial dilutions were made to provide a total of five compound concentrations plus control. Aliquots of 100 μL of these different compounds dilutions were added to the appropriate microtiter wells already containing 100 μL of medium, resulting in the required final compound concentrations.

Following tested compounds addition, the plates were incubated for an additional 48 h at 37 °C, 5 % CO_2, 95 % air, and 100 % relative humidity. For adherent cells, the assay was terminated by the addition of cold TCA. Cells were fixed *in situ* by the gentle addition of 50 μL of cold 50 % (*w/v*) TCA (final concentration, 10 % TCA) and incubated for 60 min at 4 °C. The supernatant was discarded, and the plates were washed five times with tap water and air dried. Sulforhodamine B (SRB) solution (100 μL) at 0.4 % (w/v) in 1 % acetic acid was added to each well, and plates were incubated for 10 min at room temperature. After staining, unbound dye was removed by washing five times with 1 % acetic acid and the plates were air dried. Bound stain was subsequently solubilized with 10 mM trizma base, and the absorbance was read on an automated plate reader at a wavelength of 515 nm. For suspension cells, the methodology was the same except that the assay was terminated by fixing settled cells at the bottom of the wells by gently adding 50 μL of 80 % TCA (final concentration, 16 % TCA). Using the seven absorbance measurements [time zero, (Tz), control growth, (C), and test growth in the presence of tested compound at the five concentration levels (Ti)], the percentage growth was calculated at each of the tested compound concentrations levels.

Percentage growth is calculated as:

$$[(\mathrm{Ti}-\mathrm{Tz})/(\mathrm{C}-\mathrm{Tz})] \times 100 \text{ for concentrations for which } \mathrm{Ti} > / = \mathrm{Tz}$$

$$[(\mathrm{Ti}-\mathrm{Tz})/\mathrm{Tz}] \times 100 \text{ for concentrations for which } \mathrm{Ti} < \mathrm{Tz}$$

Three dose response parameters were calculated for each experimental agent. Growth inhibition of 50 % (GI_{50}) was calculated from [(Ti-Tz) / (C-Tz)] × 100 = 50, which was the tested compound concentration resulting in a 50 % reduction in the net protein increase (as measured by SRB staining) in control cells during the compound incubation. The tested compound concentration resulting in total growth inhibition (TGI) was calculated from Ti = Tz. The LC_{50} (concentration of drug resulting in a 50 % reduction in the measured protein at the end of the drug treatment as compared to that at the beginning) indicating a net loss of cells following treatment was calculated from [(Ti-Tz) / Tz] × 100 = −50. Values were calculated for each of these three parameters if the level of activity was reached; however, if the effect was not reached or was exceeded, the value for that parameter was expressed as greater or less than the maximum or minimum concentration tested.

2.3. In vitro kinase enzyme assay

The enzymatic assays of wild type BRAF ($BRAF^{WT}$), mutated BRAF ($BRAF^{V600E}$), and CRAF were performed in Reaction Biology Corp. (http://www.reactionbiology.com) using a standard protocol and at a 1 μM ATP concentration and 3-fold dilution factor. The tested compounds were tested in 10-dose IC_{50} mode with 3-fold serial dilution starting at 0.01 or 10 μM. In a final reaction volume of 25 μL, kinase (5–10 mU) were incubated with 25 mM Tris pH 7.5, 0.02 mM EGTA, 0.66 mg/mL myelin basic protein, 10 mM magnesium acetate, and [γ33P-ATP] (specific activity approx. 500 cpm/pmol, concentration as required). The reaction was initiated by introducing the Mg-ATP mixture. Following a 40-min incubation at room temperature, the reaction was

quenched with the addition of 5 μL of 3 % phosphoric acid. Subsequently, a 10 μL aliquot of the reaction mixture was applied onto a P30 filtermat, followed by washing with 75 mM phosphoric acid (3 × 5 min) and a final wash with MeOH. The filtermat was then dried before scintillation counting.

2.4. In vitro mutated BRAF-based cell line assay

The selected compounds were tested against mutated BRAF-derived non-resistant melanoma cell line (A375), mutated BRAF-derived resistant melanoma cell line (A375R), and mutated-BRAF-derived colon cancer cell line (RKO) at College of Pharmacy (Chosun University, Republic of Korea) using MTT (3-(4,5-dimethylthiazol-2-yl)-2,5-diphenyltetrazolium bromide) assay [55] to identify the IC_{50} values using vemurafenib **I** and sorafenib **VI** as positive controls. The drug-resistant melanoma cell line (A375R) was generated by repeated exposures to increasing concentrations of vemurafenib **I** [56].

2.5. In silico molecular docking simulation

The molecular docking simulation of the designed derivatives was performed using Molecular Graphics Laboratory (MGL) Tools software suite 1.5.7 (Sanner lab, Centre for Computational Structural Biology, Scripps Research Institute). The molecular docking protocol was conducted through the following steps:

2.5.1. Ligand preparation

The chemical structures of the tested compounds were built using ChemSketch software and optimized by Discovery Studio 2021 software using Dreiding-like forcefield [57]. Gasteiger charges were applied to merge the non-polar hydrogens using AutoDock Tools 1.5.6.

2.5.2. Protein preparation

The X-ray structure of $BRAF^{V600E}$ kinase domain (PDB ID: 3OG7) was downloaded from the RCSB protein databank. Reference ligand (vemurafenib **I**), water molecules, and any additional chains were removed, keeping one chain of kinase domain only. The hydrogen atoms and Asn/Gln/His flips were assigned using Molprobity. AD4 parameters and Gasteiger charges were assigned to the protein atoms using AutoDock Tools 1.5.6.

2.5.3. Molecular docking protocol validation

Molecular docking calculations were performed using AutoDock4 using ten runs of genetic algorism (GA) at the ATP binding site coordinates (x = 1.869, y = −2.638, z = −19.918). The docking protocol was validated through running initial docking experiments (pre-docking) for the reference ligand (vemurafenib **I**) and calculating the RMSD value. The molecular docking of the designed compounds was conducted, and the most stable conformational clusters were identified.

2.5.4. Molecular docking analysis

The docking poses of the tested compounds were visualized and analyzed using Discovery Studio software 2021 to identify potential binding modes and the possible binding interactions between the docked ligands and the key amino acid residues at the ATP binding site of $BRAF^{V600E}$ kinase domain.

2.6. Immunoblotting assay

The selected compound, **KS16**, using vemurafenib **I** as standard, was tested using immunoblotting assay within melanoma cell lines (sensitive type and resistant form, A375 and A375R, respectively). The melanoma cell lines were treated with the tested compound, KS16, and vemurafenib **I** at two different concentrations (0.1 and 1 μM) for 24 h and immunoblotted with antibodies against phospho-MEK1/2, phospho-ERK1/2, ERK, and MEK, respectively. Dose-dependent inhibition is noticed in western blotting of both compounds against phospho-MEK1/2, phospho-ERK1/2.

2.7. In vitro kinase panel assay

Kinase-tagged T7 phage strains were cultured in parallel using 24-well blocks with an *E. coli* host derived from the BL21 strain. The *E. coli* was grown to log-phase, then infected with T7 phage from a frozen stock (multiplicity of infection = 0.4) and incubated at 32 °C with shaking until lysis occurred (90–150 min). The lysates were clarified by centrifugation at 6000 *g* and filtration through a 0.2 μm membrane to remove cellular debris. Kinases were subsequently expressed in HEK-293 cells and tagged with DNA for quantitative PCR (qPCR) detection. Streptavidin-coated magnetic beads were incubated with biotinylated small molecule ligands for 30 min at room temperature, generating affinity resins for kinase assays. The liganded beads were blocked with excess biotin and washed with blocking buffer (SeaBlock (Pierce), 1 % BSA, 0.05 % Tween 20, 1 mM DTT) to eliminate unbound ligands and minimize non-specific phage binding. Binding reactions were prepared by mixing kinases, ligand-coated affinity beads, and test compounds in 1× binding buffer (20 % SeaBlock, 0.17× PBS, 0.05 % Tween 20, 6 mM DTT). Test compounds were prepared as 40× stocks in 100 % DMSO and diluted directly into the assay. All reactions were carried out in polypropylene 384-well plates, with a final reaction volume of 0.04 mL. The assay plates were incubated at room temperature with shaking for 1 h, after which the affinity beads were washed with wash buffer (1× PBS, 0.05 % Tween 20). The beads were then re-suspended in elution buffer (1× PBS, 0.05 % Tween 20, 0.5 μM non-biotinylated affinity ligand) and incubated with shaking at room temperature for 30 min. The kinase concentrations in the eluates were subsequently quantified *via* qPCR.

2.8. In vivo antitumor evaluation

The selected compound (**KS16**) was evaluated to inhibit the tumor growth in the animal model. The animal model was generated using A375 melanoma xenograft in male BALB/c nude mice (hairless and albino 6 weeks old animal, with lack of thymus, was unable to produce T-cells, therefore they were immunodeficient) using vemurafenib **I** (group 2) and **HM95574** (group 3) as standards and saline (group 1) as a negative control. The selected candidate (**KS16**) was IP injected once every other day to two groups of mice (group 4 and 5) in two different doses (25 and 50 mg/kg, respectively). Tested mice were obtained from Orient (Seongnam, Republic of Korea) and maintained in cages in a light- and temperature-controlled room. A375 cells were subcutaneously injected (2×10^6 cells) into the left flank of mice. After 5 days, the mice were randomly divided into different groups ($N = 8$). Mice were intraperitoneally injected with saline, or tested compound (vemurafenib **I**, **HM95574**, or **KS16**) three times each week. The four groups were monitored for 25 days. The animals were kept under controlled weather and feeding conditions, and tumor volume (mm^3) was calculated, and weight (g) measured for all groups, our selected candidate (**KS16**), standards (vemurafenib **I** and **HM95574**) and negative control (saline), to evaluate the effects of **KS16**. Tumor diameters were measured using calipers (Mitutoyo, Kawasaki, Japan) and the volume was calculated as follows: Tumor volume = 0.5 × [(large diameter) × (small diameter)^2]. All animal care and experimental procedures complied with local guidelines and were approved by the Animal Experiments Committee of Chosun University (approval number: CIACUC 2020-S0022).

2.9. Normal cell cytotoxicity assay

The MTT (3-(4,5-dimethylthiazol-2-yl)-2,5-diphenyl tetrazolium bromide) assay, originally developed by Mosmann and later modified by Miura, was employed to assess the *in vitro* inhibitory effects of the tested compounds (**22b**, **22c**, and **KS16**) on cell growth. BJ1 cells (10×10^3 cells per well) were seeded into a 96-well microplate in fresh complete

growth medium. The test compounds were added simultaneously to triplicate wells, and the final volume was adjusted to 100 μL. The plate was incubated for 72 h at 37 °C in a humidified atmosphere of 5 % CO_2 using a water-jacketed carbon dioxide incubator (TC2323; Sheldon, Cornelius, OR). Following incubation, the medium was removed, fresh serum-free medium was added, and cells were treated with varying concentrations of the compounds (500, 100, 50, 25, 12.5, 6.25, 3.125, and 0.78 mg/mL). Cells were suspended in DMEM-F12 supplemented with 1 % antibiotic-antimycotic mixture (10,000 U/mL potassium penicillin, 10,000 mg/mL streptomycin sulfate, and 25 mg/mL amphotericin B) and 1 % L-glutamine, then incubated at 37 °C under 5 % CO_2 for 48 h. After incubation, the medium was aspirated, and 200 μL of 10 % sodium dodecyl sulfate (SDS) in deionized water was added to each well and incubated overnight at 37 °C under 5 % CO_2. The reaction was stopped by the addition of 200 μL of 10 % SDS in deionized water, followed by overnight incubation at 37 °C to solubilize the MTT formazan. To further solubilize the formazan, 100 μL of 0.02 N HCl in 50 % *N,N*-dimethylformamide and 20 % SDS was added to each well. The optical density (OD) of each well was measured at 575 nm using a microplate reader (model 3350; Bio-Rad Laboratories Inc., Hercules, CA). The percentage of cell growth inhibition was calculated as (1 - T/C) × 100, where C is the mean OD575 of the control group and T is the OD575 of the treated group. The IC50 values were determined from the dose-response curves.

2.10. hERG binding assay

The assay was conducted at Medivalley, Daegu-Gyeongbuk Medical Innovation Foundation, Republic of Korea using hERG Fluorescence Polarization Assay (Invitrogen: PV5365) using Synergy Neo (Biotek). When a fluorescent hERG channel tracer binds to a membrane containing hERG channel protein, the rotation of the tracer was restricted, resulting in a high degree of polarization. However, when a competitive inhibitor binds to the hERG channel, the tracer was competitively displaced from the membrane, losing its directionality and resulting in loss of polarization. Compound E-4031, positive control, was diluted stepwise by 3-fold and mixed with pre-prepared membranes containing hERG channels and fluorescent tracers. After incubating for about 4 h, the polarization values were measured at various concentrations to calculate the IC_{50}. For the tested compound, **KS16**, fluorescence intensity was measured at 16 points of diluted concentrations (excitation at 530 nm, Emission at 590 nm) and compared with the DMSO solvent control.

2.11. In vivo pharmacokinetic profiling

KS16 was selected to be evaluated for its *in vivo* pharmacokinetic profile along with additional two compounds among the same potent series (series B; **22b** and **22c**) at Drug Discovery Platform Team (Korea Research Institute of Chemical Technology, Republic of Korea). The animal study was approved by the Institutional Animal Care and Use Committee (IACUC) of the Korea Research Institute of Chemical Technology (IACUC No. 2023-7F-10-01). Six male ICR mice were sourced from OrientBio (Sungnam, South Korea) to conduct the *in vivo* PK profiling. The tested compounds were administered *via* two routes (IV, 5 mg/Kg and PO, 10 mg/kg) to evaluate the plasma concentration curve and to measure the pharmacokinetic parameters for both IV and PO administration. The lowest quantification limit in the analysis method for the tested compounds 0.5 ng/mL. The composition of the administration solvent was DMSO: PEG400: DW =5: 40: 55 (5 mL/kg) for the conducted experiments. Animal conditions remained normal throughout the duration of the PK experiment, with no specific observations noted. Values detected below the quantification limit are denoted as BQL (Below Quantification Limit) and have been excluded from the profile. Blood samples are collected at predetermined times after administering the tested compound to 7–9-week-old ICR mice that have undergone an acclimatization period. The supernatant after centrifugation (13,000 rpm, 4 °C, 10 min) was analyzed by LC-MS/MS. Mass spectrometry (Agilent 6460) with HPLC (Agilent 1260) was used in the analytical method. For calibration curve samples (0.5–8000 ng/mL), a tenfold higher concentration solution was prepared in blank plasma and processed using the same method as the tested compounds. The analysis is performed using the Phoenix WinNonlin (Pharsight ver 6.4, USA) non-compartmental analysis model. [58]

2.12. Microsomal stability

Human liver microsomes (0.5 mg/mL) was treated with **KS16** in 1 μM concentration and mixed with 0.1 M phosphate buffer (pH 7.4). After pre-incubating for 5 min at 37 °C, the NADPH Regeneration system solution was added, and the mixture was cultured for 30 min at 37 °C. Internal standard (chlorpropamide) solution in MeCN was added followed by centrifugation for 5 min at 14,000 rpm and 4 °C to terminate the reaction. The supernatant was injected into the LC-MS/MS system to evaluate the metabolic stability of **KS16** by analyzing the substrate drug. The remaining amount of substrate was analyzed using the Shimadzu Nexera XR system and TSQ vantage (Thermo) after the reaction. A Kinetex C18 column (2.1 × 100 mm, 2.6 μm particle size; Phenomenex) was used as the HPLC column. The mobile phase consisted of distilled water containing 0.1 % formic acid (A) and acetonitrile containing 0.1 % formic acid (B). Data analysis was performed using Xcalibur (version 1.6.1) [58,59].

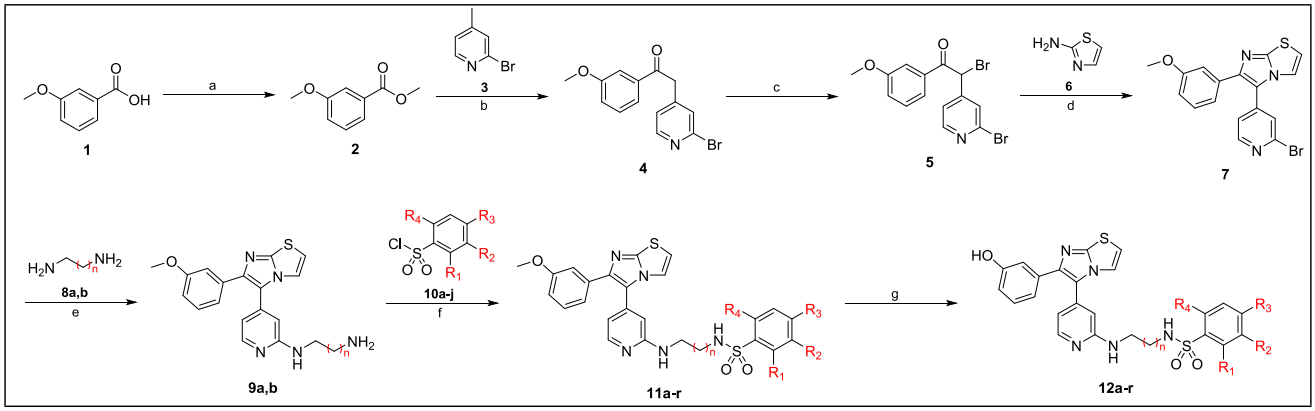

Scheme 1. Synthetic route of pyridine derivatives (series A: **11a-r** and **12a-r**). Reagents and conditions: **a**, MeOH, conc. H_2SO_4, reflux, 18 h; **b**, LiHMDS, THF, −78 °C – rt., 1.5 h; **c**, NBS, DMF, 60 °C, 3 h: **d**, MeCN, reflux, 18 h; **e**, Reflux, 30 h; **f**, Et_3N, DCM, 0 °C – rt., 6 h; **g**, BBr_3, DCM, −10 °C – rt., 6 h.

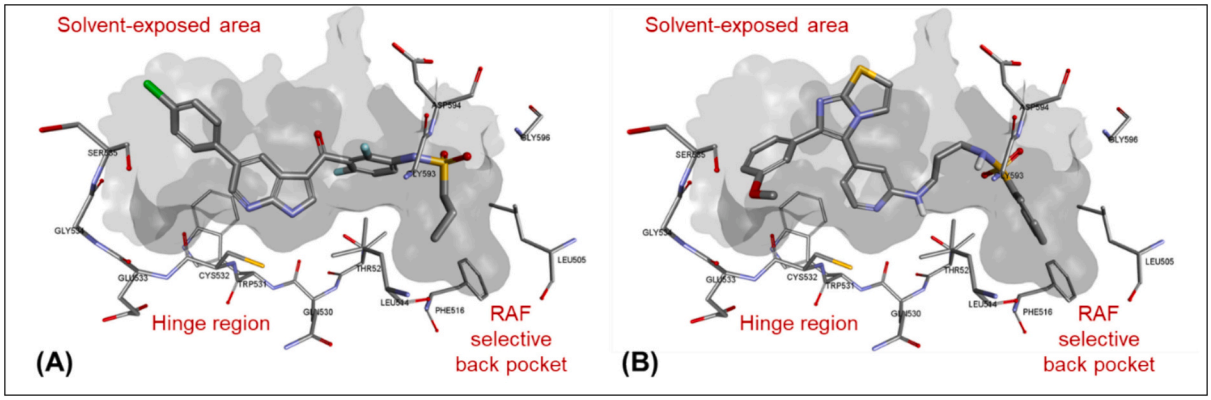

Fig. 3. 3D binding interaction of vemurafenib **I** (**A**) and compound **11b** (**B**) into the ATP binding site of BRAF^{V600E} kinase domain (PDB ID: 3OG7). **A**, the azaindole core scaffold of vemurafenib **I** anchored to the hinge binding region to interact with Cys 532 by HB interaction. The terminal propyl group anchored to the RAF selective back pocket, but it could not fully access into this space to provide key hydrophobic interactions. The distal chlorophenyl ring directed to the solvent-exposed area; **B**, the central pyridine ring of compound **11b** oriented in the hinge region to provide HB interaction with Thr 529. The terminal unsubstituted ring of compound **11b** occupied into the RAF selective back pocket to provide additional hydrophobic interactions, compared to that of vemurafenib **I**. The core imidazothiazole and the distal phenyl ring were anchored to the solvent exposed area.

2.13. CYP450 inhibition assay

Human liver microsomes (0.25 mg/mL) were mixed with 0.1 M of phosphate buffer solution (pH 7.4) and a substrate drug cocktail of five drug-metabolizing enzymes (Phenacetin 50 μM, Diclofenac 10 μM, S-mephenytoin 100 μM, Dextromethorphan 5 μM, Midazolam 2.5 μM), along with tested compounds (**22c** and **KS16**) at concentrations of 0 and 10 μM. The mixture was pre-incubated at 37 °C for 5 min. Then, an NADPH generation system solution was added, and the mixture was further incubated at 37 °C for 15 min. Internal standard substance (Terfenadine) solution in MeCN was added to terminate the reaction. After centrifugation for 5 min (at 14,000 rpm, 4 °C), the supernatant was injected into the LC-MS/MS system to simultaneously analyze the metabolites of the substrate drugs. This procedure was employed to evaluate the inhibitory activity of the two compounds on drug-metabolizing enzymes. The metabolites of each CYP enzyme indicator drug generated through the reaction were analyzed using the Shimadzu Nexera XR system and TSQ vantage (Thermo). An HPLC column of Kinetex C18 (2.1 × 100 mm, 2.6 μm particle size; Phenomenex, USA) was employed, with a mobile phase consisting of 0.1 % formic acid in distilled water (A) and 0.1 % formic acid in acetonitrile (B). The gradient flow increased from 0%B in A to 50 % B in A in a period of 4 min in flow rate 0.3 mL/min. The generated metabolites were quantified using Multiple Reaction Monitoring (MRM) mode, and data analysis was performed using Xcalibur (version 1.6.1) [58,60,61].

3. Results and discussion

3.1. Design of the initial series (series A)

In the current study, we have set up an optimized and more sustainable synthetic route to the final target compounds, compared to that of the synthetic scheme in our previous work [53], where we did not include the palladium-catalysed reaction and improved the yield across the steps within the settled synthetic scheme. The designed compounds of Series A were synthesized and purified using the depicted Scheme 1. Methyl benzoate derivative (**2**, good leaving group containing compound for the synthetic transformation reaction) was afforded by Fisher esterification between benzoic acid derivative (**1**) and methanol in presence of catalytic amount of dehydrating agent (conc sulfuric acid). The ketide intermediate (**4**) was synthesized *via* carbon-carbon bond formation between methyl ester, good leaving group, of compound **2** and 4-methyl group of pyridine derivative **3** using lithium bis(trimethylsilyl)amide as a strong non-nucleophilic base to deprotonate the acidic proton of 4-methyl group of pyridine derivative **3** (nucleophilic substitution reaction) [62]. Bromination of α carbon of ketide derivative **4** was conducted using *N*-bromosuccinimide (NBS) to afford α bromo ketone derivative **5**. The key intermediate (**7**, imidazothiazole-based scaffold) was achieved *via* coupling and cyclization reaction between α bromo ketone-based derivative **5** and 2-aminothiazole **6**. Nucleophilic aromatic substitution reaction (SNAr) was conducted between the key intermediate **7** and different diamines to afford compounds **9a,b**. Coupling between NH_2-bearning compounds (**9a,b**) with different substituted benzenesulfonyl chloride was achieved *via* Hinsberg reaction in presence of triethylamine (Et_3N) as base to give the final target compounds **11a-r**. Additional final target compounds (**12a-r**) were afforded *via* demethylation of compounds **11a-r** using boron tribromide as strong Lewis acid (Table 1).

Initially, two compounds were designed (**11a,b**) with terminal unsubstituted phenyl group to test the antiproliferative activities of the designed compounds in the current study with different spacer lengths; two-carbon spacer (**11a**) and three-carbon spacer (**11b**). These two compounds were docked into the ATP binding site of BRAF^{V600E} kinase domain (Fig. 3). They showed the same binding mode of the reference ligand (vemurafenib **I**, FDA-approved BRAF^{V600E} inhibitor). The molecular docking revealed that the designed compounds exhibited patterned binding poses within the ATP binding site of BRAF^{V600E} kinase domain. Where, the central pyridine ring was allocated within the hinge segment to afford HB interaction with Thr 529. Additionally, the terminal phenyl ring was anchored to the RAF selective back pocket and perfectly fitted (in contrast to vemurafenib **I** that anchored a terminal propyl group to this iconic room providing weak hydrophobic interactions, Fig. 3A) to provide a number of hydrophobic interactions with the key amino acid residues within this pocket (Leu 505, Leu 514, Phe 516, Ile 527, Gly 593, and Phe 595). The spacer between the hinge binding motif and the terminal phenyl ring, with HBDs and HBAs, was aligned along the activation loop to afford strong HB interactions with the key amino acid residues at this site (Asp 594 and Gly 596). Moreover, both core imidazothiazole ring and the distal phenyl ring with OMe group were directed to the solvent exposed area to afford key binding with the amino acid residues at this site (Ala 481, Trp 531, and Phe 583). In compound **11a** (two-carbon spacer), it was noted that the attraction of the terminal phenyl ring into the RAF selective back pocket shifted the hinge binding motif (pyridine ring) slightly away from the hinge segment. However, by expanding the spacer between the terminal phenyl ring and the central pyridine hinge binding motif with three-carbon linker (compound **11b**), it pushed the central ring to be allocated closely into the hinge segment to afford key HB interactions

Table 2
In vitro cytotoxicity assay of the tested compounds **11a-r** against NCI melanoma cell lines (leukemia, non-small cell lung cancer, colon cancer, CNS cancer, melanoma, ovarian cancer, renal cancer, prostate cancer, breast cancer cell lines) expressed in mean growth %.

Compound	Mean growth %	Compound	Mean growth %
11a	26.1 %	**11j**	41.7 %
11b	34.2 %	**11k**	81.8 %
11c	39.9 %	**11l**	63.8 %
11d	52.8 %	**11m**	33.3 %
11e	98.4 %	**11n**	16.2 %
11f	43.8 %	**11o**	47.6 %
11g	24.6 %	**11p**	36.2 %
11h	24.0 %	**11q**	61.0 %
11i	80.8 %	**11r**	61.5 %

with hinge amino acid residues (Fig. 3B).

Additionally, a group of compounds were designed in order to evaluate their inhibitory activities through the ligand expansion by introducing different functional groups into the terminal phenyl ring across the 2-carbon and 3-carbon spacers. The terminal phenyl ring was decorated with different hydrophobic groups (**11c-r**) to identify the impact of these substitutions around the terminal phenyl ring on the inhibitory activities. These derivatives were docked into the binding site of $BRAF^{V600E}$ kinase enzyme to explore any additional binding interactions between the key amino acids at the RAF selective back pocket and the newly introduced functional groups. The molecular docking results revealed that the decoration of the terminal phenyl ring with different substitutions has substantial influence on the binding of this binding motif into the RAF selective back pocket. Where, the substitution with fluoro (**11g,h,m,n**) and chloro (**11i,j,o,p**) groups around this hydrophobic motif allowed this motif to exist in this iconic pocket. However, by expanding the size of these substitutions with large groups such as CF_3 (**11c,d**), OMe (**11e,f**) and Br (**11*k,l***), the size of the terminal motif become more bulky to be tolerated in this space allowing this terminal motif to suited away from the key hydrophobic amino acid residues within the RAF selective back pocket. For compounds with the ortho-disubstitution (**11q,r**), the terminal phenyl ring lost its planarity with the core structure of these derivatives and they did not exhibit the patterned binding mode across the designed derivatives (series A).

In vitro cytotoxic evaluation was conducted to evaluate their anti-proliferative activities over NCI human cancer cell lines (Table 2, melanoma cell lines; and **Figs. S1–20**). The results revealed that the compounds should different cytotoxic activities across the NCI human cancer cell lines (leukemia, non-small cell lung cancer, colon cancer, CNS cancer, melanoma, ovarian cancer, renal cancer, prostate cancer, breast cancer cell lines). In addition, the size of the newly incorporated groups affects the anti-proliferative activities. The cytotoxic activity increases as the size of the group decrease (F; **11g,h** > CF_3; **11c,d** > Cl; **11i,j** > Br; **11k,l** > OMe; **11e,f**). For the small-sized substitutions (compounds **11a,h,m,n** with F group) showed comparable inhibitory activities with that of corresponding unsubstituted terminal phenyl derivatives (**11a,b**). These comparable results may be referred to the similar size of fluorine atom in **11g,h,m,n** and hydrogen atom in **11a,b**. The results showed that the terminal phenyl ring can tolerate the small-sized groups only (H and F, Cl) compared to the larger-sized chemical moieties (CF_3, OMe, and Br). Generally, the axial ligand expansion did not improve the antiproliferative effect of the design compounds. Furthermore, the results revealed that the RAF selective back pocket has a limited volume to be fitted with 6-membered aromatic ring. It was noted that the F-substituted derivatives showed better cytotoxic activities compared to that of unsubstituted derivatives. Aligned with the results from the molecular docking studies, it was concluded that the introduced F group in the designed compounds exhibited additional binding interactions with the key amino acid residues within the RAF selective back pocket (halogen interaction with Ile 592).

Table 3
In vitro kinase inhibitory biochemical assay results (Inh%) of the tested compounds **11a-r** against $BRAF^{V600E}$ kinase enzyme.

Compound	$BRAF^{V600E}$ Inh%	Compound	$BRAF^{V600E}$ Inh%
11a	97.1 % (IC_{50} = 1.3 μM)	**11j**	93.2 %
11b	96.9 % (IC_{50} = 1.9 μM)	**11k**	88.1 %
11c	88.2 %	**11l**	92.3 %
11d	94.7 %	**11m**	96.2 %
11e	91.2 %	**11n**	96.5 %
11f	91.4 %	**11o**	94.0 %
11g	89.7 %	**11p**	87.3 %
11h	91.5 %	**11q**	91.0 %
11i	90.0 %	**11r**	92.2 %

To validate the $BRAF^{V600E}$ kinase as the potential biological target for the tested compounds **11a-r**, *in vitro* kinase inhibitory biochemical assay was conducted for the tested compounds against $BRAF^{V600E}$ to evaluate their inhibitory activities (Table 3). The results revealed that the tested compounds exhibited different range of inhibitory activities. The results showed potent inhibitory activities of both compounds **11a, b** with IC_{50} 1.3 and 1.9 μM, respectively.

A set of analogues of all tested derivatives in this current study with OH-bearing phenyl group at the solvent-exposed binding motif was designed and synthesized (**12a-r**, Table 1 and Scheme 1) to investigate the influence of both polarity (TPSA), on *in vitro* cellular assay, and the newly introduced HBD group (OH) on the binding affinity in *in vitro* $BRAF^{V600E}$ kinase assay. The *in silico* molecular docking of the new designed candidates showed that most of the compounds exhibited the same binding mode of OMe-based candidates (**11a-r**) showing the terminal phenyl ring into the RAF selective back pocket, for the unsubstituted and small-sized substituted derivatives, and the central pyridine ring oriented at the hinge segment within the ATP binding site. It was interesting to explore that the distal phenyl ring, with the naked hydroxy group, anchored to the solvent-exposed area. Additionally, this distal phenyl ring was rotated, across the synthesized derivatives **12a-o**, to anchor the OH group close to the key amino acid residue within the hinge region (Cys 532) to form strong HB interaction (Fig. 4). Generally, the new synthesized compounds showed additional interactions within the ATP binding site that predict the improved potency profile of this series (**12a-o**). However, the *in vitro* cytotoxic assay showed poor cytotoxic activities of OH-bearing compounds (**12a-r**) compared to OMe-bearing derivatives (Table 4 and **Table S19–31**). The week cytotoxic activities of the new designed compounds could be explained by the poor cellular induction due to the high values of TPSA (**12a** $_{TPSA}$ = 106.39 $Å^2$) in contrast to the appropriate TPSA of OMe-bearing derivatives (**11a** $_{TPSA}$ = 95.39 $Å^2$) which showed outstanding cytotoxic activities over NCI human cancer cell lines (leukemia, non-small cell lung cancer, colon cancer, CNS cancer, melanoma, ovarian cancer, renal cancer, prostate cancer, breast cancer cell lines). The unsubstituted terminal phenyl derivatives (**12a,b**) and F-substituted phenyl derivatives (**12h,n**), whose OMe analogues showed potent *in vitro* results, were selected for 10 point kinase assay to determine the IC_{50} values (Table 5). The results showed that the new compounds exhibited potent inhibitory activities (IC_{50} 0.04 and 0.07 μM for **12a** and **12b**, respectively) compared to OMe-bearing derivatives (IC_{50} 1.3 and 1.9 μM for **11a** and **11b**, respectively). The *in silico* molecular docking along with the *in vitro* kinase assay revealed that the newly incorporated HBD group (OH) enhanced the kinase inhibitory activities by 30-folds due to additional binding affinities. However, this incorporated polar group is not sufficient to adapt these small molecule candidates into the cancer cell.

For further exploration of the cytotoxic effect of series A compounds against mutated BRAF-bearing melanoma cell line, the *in vitro* cell-based cytotoxicity assay was conducted for the selected compounds using vemurafenib **I** as positive control (Table 6). The results revealed that all the tested compounds showed weaker inhibitory activities against melanoma cell line (A375) compared to the reference compound

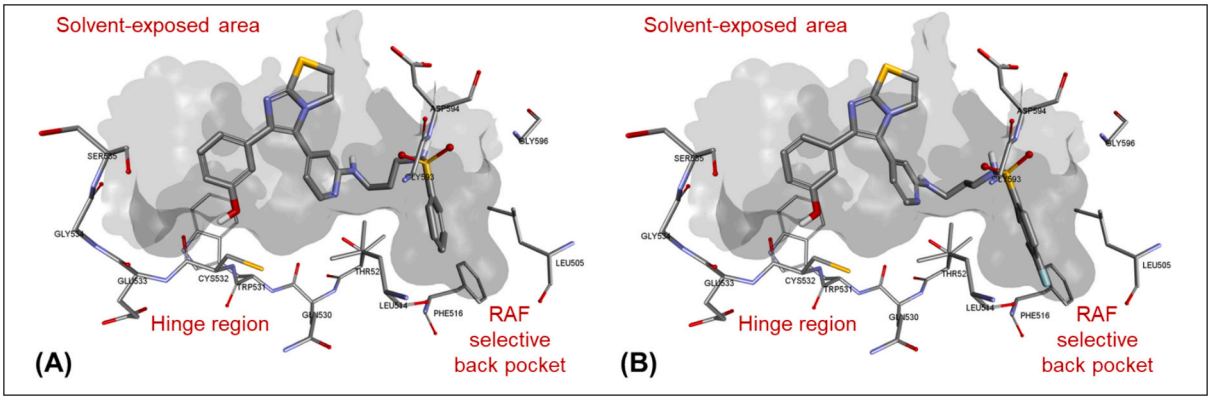

Fig. 4. 3D binding interaction of OH-bearing derivatives (compound **12b**, **A**; and compound **12h**, **B**) into the ATP binding site of BRAF^{V600E} kinase domain (PDB ID: 3OG7). The distal phenyl ring of both compound **11b** and **12h** rotated to direct the naked hydroxyl group (HBD) close to Cys 532 affording strong HB interactions (**A** and **B**). The terminal 4-fluorophenyl group of compound **12h** is perfectly fitted into the RAF selective back pocket affording additional halogen interaction with Ile 592 (**B**).

Table 4
In vitro cytotoxicity assay of the new tested compounds **12a-r** against NCI melanoma cell lines (leukemia, non-small cell lung cancer, colon cancer, CNS cancer, melanoma, ovarian cancer, renal cancer, prostate cancer, breast cancer cell lines) expressed in mean growth %.

Compound	Mean growth %	Compound	Mean growth %
12a	74.8 %	**12j**	95.5 %
12b	38.1 %	**12k**	62.5 %
12c	37.2 %	**12l**	69.6 %
12d	ND[a]	**12m**	70.3 %
12e	95.0 %	**12n**	82.1 %
12f	ND	**12o**	45.4 %
12g	66.9 %	**12p**	45.7 %
12h	81.4 %	**12q**	61.3 %
12i	68.4 %	**12r**	60.9 %

[a] ND, not determined.

Table 5
IC_{50} values (μM) of compounds **12a,b,h,n** against BRAF^{V600E} kinase enzyme.

Compound	IC_{50} (μM)[a]	Compound	IC_{50} (μM)[a]
12a	0.04 ± 0.02	**12h**	1.26 ± 0.04
12b	0.07 ± 0.01	**12n**	0.83 ± 0.01

[a] The standard deviation values were calculated from duplicate assays.

Table 6
In vitro cytotoxic assay data (IC_{50}) of selected compounds over BRAF^{V600E}-bearing melanoma cell line (A375).

Compound	IC_{50} value (μM)[a]	Compound	IC_{50} value (μM)[a]
11a	6.36 ± 0.98	**11q**	8.94 ± 1.99
11i	11.11 ± 1.33	**12a**	8.27 ± 1.82
11k	11.64 ± 1.05	**12n**	11.59 ± 4.01
11l	11.59 ± 0.32	**12q**	11.67 ± 2.88
11n	4.70 ± 0.89	Vemurafenib **I**	0.59 ± 0.31
11p	8.25 ± 2.23		

[a] The standard deviation values were calculated from triplicate assays.

(vemurafenib, IC_{50} 0.59 μM). Interestingly, compound **11n** (3-F substituted derivative with 3-carbon spacer) showed the most potent activity (IC_{50} 4.70 μM) among the tested compounds. The results showed the significant effect of F group in inhibition of BRAF^{V600E} kinase enzyme.

Table 7
The key structure of the new designed compounds (series B) and IC_{50} values (nM) against BRAF^{V600E} protein kinase.

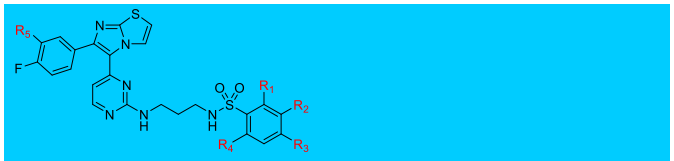

Compound	R_1	R_2	R_3	R_4	R_5	IC_{50} (nM)[a]
21a	H	F	H	H	OMe	1.93 ± 0.31
21b	H	H	H	H	OMe	3.22 ± 0.92
21c	H	H	Me	H	OMe	2.73 ± 0.08
21d	H	H	CF_3	H	OMe	1.81 ± 0.15
21e	H	H	Cl	H	OMe	ND[b]
21f	H	H	Br	H	OMe	ND
21 g	H	H	F	H	OMe	1.66 ± 0.30
21 h	Cl	H	H	Cl	OMe	3.77 ± 0.25
22a	H	F	H	H	OH	0.51 ± 0.07
22b	H	H	H	H	OH	0.34 ± 0.02
22c	H	H	Me	H	OH	0.28 ± 0.03
22d	H	H	CF_3	H	OH	0.34 ± 0.06
22e	H	H	Cl	H	OH	0.56 ± 0.02
22f	H	H	Br	H	OH	0.51 ± 0.07
22 g (KS16)	H	H	F	H	OH	0.26 ± 0.01
22 h	Cl	H	H	Cl	OH	1.23 ± 0.03
Vemurafenib **I**	–	–	–	–	–	25.15 ± 4.21

a: The standard deviation values were calculated from duplicate assays.
b: ND, not determined.

3.2. Design and development of optimized compounds (series B)

As a group, we have decided to pursue additional drug developments and further modifications of imidazothiazole-based derivatives taking this compound (**11n**) as a lead compound. A new set of compounds (series B) has been designed and synthesized (Table 7 and Scheme 2). In this series, at the hinge binding motif, the pyridine ring was replaced with pyrimidine ring to identify the possibility of additional binding interactions to the hinge region of ATP binding site of BRAF^{V600E} kinase domain. In addition, the optimum number of carbon atoms in the linker was incorporated across the entire series (three-carbon spacer) and the same diversity of substitutions at the terminal phenyl ring was engaged in the designed series to maintain the binding of this motif into the RAF selective back pocket. Moreover, the distal phenyl ring (right-handed

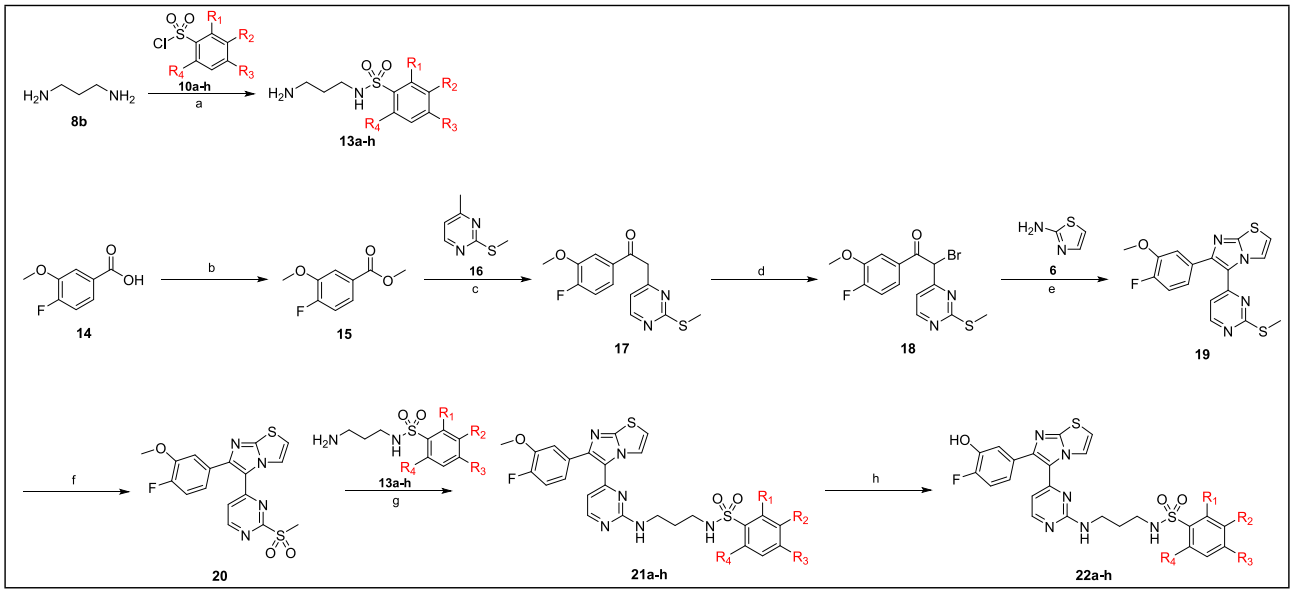

Scheme 2. Synthetic route of fluorine-bearing derivatives (series B: **21a-h** and **22a-h**). Reagents and conditions: **a**, Et_3N, DCM, 0 °C – rt., 18 h; **b**, MeOH, conc. H_2SO_4, reflux, 18 h; **c**, LiHMDS, THF, −78 °C – rt., 1.5 h: **d**, NBS, DCM, rt., 30 min; **e**, MeCN, reflux, 18 h; **f**, Oxone, MeOH/H_2O, rt., 48 h; **g**, DIPEA, DMSO, 90 °C, 9 h; **h**, BBr_3, DCM, −10 °C – rt., 6 h.

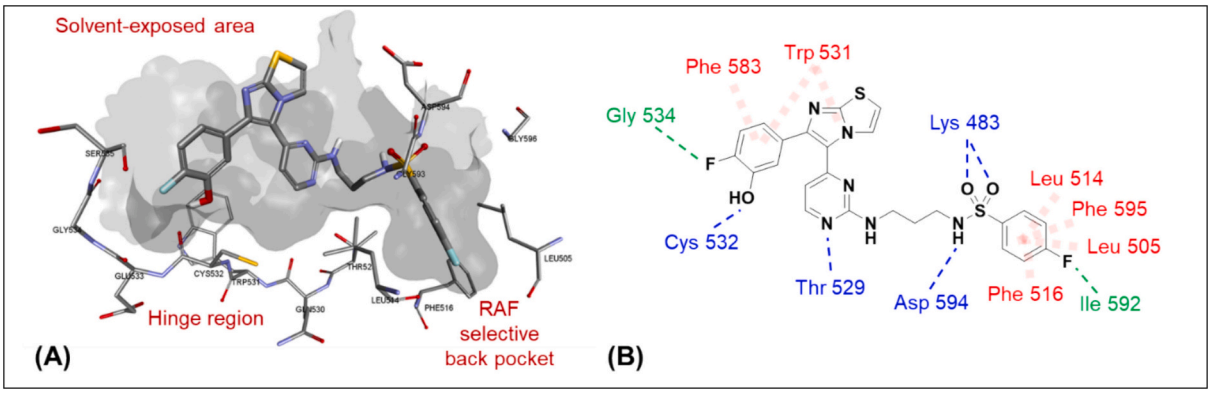

Fig. 5. *In silico* molecular docking results of **KS16** (**22g**) into the ATP binding site of $BRAF^{V600E}$ kinase domain (PDB ID: 3OG7). **A**, the 3D binding interaction showing both fluorine groups at position 4 at both terminal and distal phenyl ring anchoring the RAF selective back pocket (Leu 505 – Val 528); **B**, the 2D interaction showing the key binding interactions of core motifs within **KS16** (blue, HB interactions; green, halogen interactions; red, hydrophobic interactions).

phenyl ring) was decorated with additional F group to enhance the lipophilicity of this new series to improve the cellular induction in the *in vitro* cytotoxicity assay. Additionally, to identify the possible interaction of this hydrogen-like-sized atom with the key amino acid residues in the ATP binding site of $BRAF^{V600E}$ protein kinase domain.

The synthetic route of series B compounds (Scheme 2) followed the same synthetic protocol of Scheme 1. Where, esterification reaction, ketide intermediate formation, bromination reaction, coupling and cyclization reaction, and demethylation reaction were carried out to afford compounds **15**, **17**, **18**, **19**, and **22a-h**, respectively. However, the thiomethoxy group (OMe) of pyrimidine-based building block (**19**) was oxidized using oxone to afford the good leaving group (methyl sulfone-based compound **20**. Additionally, the side chains (terminal phenyl group with the open chain sulfonamide) were pre-synthesized to afford compounds **13a-h** before coupling with the key intermediate **20** *via* nucleophilic aromatic substitution reaction (SNAr) in presence of organic base (*N*,*N*-diisopropylethylamine) to afford the final compounds **21a-h**.

The new synthesized compounds (series B) were tested initially against $BRAF^{V600E}$ kinase enzyme to identify the IC_{50} values using vemurafenib **I** as a positive standard (Table 7). The tested compounds showed potent IC_{50} values in nanomolar level against $BRAF^{V600E}$ protein kinase compared to the monosubstituted distal phenyl-based derivatives (series A, initial designed candidates). Surprisingly, the *in vitro* kinase assay results revealed that the hydroxyl-based derivatives (**22a-h**) enhanced the activity (0.26–0.56 nM) compared to vemurafenib **I** (25.15 nM) by 80 folds. Interestingly, compound **22g** (**KS16**; the fluorinated analogue of compound **12h**; one of the most active compounds in the initial designed series, series A) showed the most potent activity among the tested compounds (0.26 nM). It is suggested that the terminal 4-fluorophenyl ring together with the three-carbon spacer showed a significant effect in the binding onto the RAF selective back pocket of ATP binding site of $BRAF^{V600E}$ kinase domain. In addition, the central pyrimidine ring may contribute to a suitable chemical environment that allow this motif to afford an additional H bonding at the hinge region of the active site. Furthermore, the fluorine group at the distal phenyl ring (left-hand side) may afford a strong halogen binding interaction with the key amino acid residues at the solvent-exposed area of the ATP active site of $BRAF^{V600E}$ kinase domain (Fig. 5).

Table 8
The mean GI_{50} values (μM) of **KS16** against NCI 60 human cancer cell lines.

NCI human cancer cell line	Mean GI_{50} μM	NCI human cancer cell line	Mean GI_{50} μM
Leukemia	1.74	Ovarian cancer	2.77
Non-small cell lung cancer	2.41	Renal cancer	2.88
Colon cancer	2.45	Prostate cancer	2.39
CNS cancer	2.96	Breast cancer	2.20
Melanoma	0.43		

3.3. *Evaluation of most active compound **22g** (KS16)*

Compound **22g** (we will refer to it from now on with its chemist code, **KS16**; the most active compound among the designed and tested compounds in series B) was selected to be biologically evaluated further to investigate its drug-like properties to be a promising drug candidate in the treatment of the drug-resistant melanoma.

3.3.1. *In vitro cytotoxicity against NCI human cancer cell lines*

National Cancer Institute (NCI) selected **KS16** to be tested and evaluated against NCI 60 human cancer cell lines (leukemia, non-small cell lung, colon, CNS, melanoma, ovarian, renal, prostate and breast lung cancer) in five-point assay to calculate its GI_{50} values against these cancer cell lines (Table 8, Fig. 6, and **Figs. S34,35**). **KS16** showed different GI_{50} values in micromolar level against the tested human cancer cell lines. In addition, it showed better inhibitory activity compared to the initial designed series (series A, monosubstituted distal phenyl-based derivatives). It is suggested that the additional fluorine group at position 4 in the distal phenyl ring together with the central pyrimidine ring have a significant impact on modulating the lipophilicity of the compound and hence the Log *P* value to enhance the cellular induction. Furthermore, the results revealed that the human melanoma cell lines were the most sensitive cell lines (mean GI_{50} 0.43 μM) among the tested human cancer cell lines (mean GI_{50} values 1.74–2.96 μM) that reflect the selectivity of **KS16** to melanoma cell line (in contrast to the initial series, series A, that showed different cytotoxicity across NCI human cancer cell lines). This may suggest the high selectivity index of **KS16** to melanoma cell line over the other types of human cancer cell lines.

3.3.2. *In silico molecular docking simulation*

Based on *in silico* molecular docking studies, as well as *in vitro* biochemical and cell-based evaluations of both Series A and Series B, a brief structure-activity relationship (SAR) analysis was discussed and proposed by the group. It was highlighted that incorporating a new hydrogen bond acceptor (HBA) within the hinge-binding motif, specifically, a pyrimidine ring in Series B as opposed to a pyridine ring in Series A, enhances ATP-competitive inhibition by facilitating an additional strong hydrogen bond (HB) at the active site of the target protein ($BRAF^{V600E}$). Additionally, the length of the flexible open-chain spacer between the terminal phenyl ring (RAF selective back pocket binding motif) and the hinge-binding motif significantly influences the binding affinity and potency of the designed derivatives. A three-carbon spacer was found to be superior to a two-carbon spacer, as it ensures the

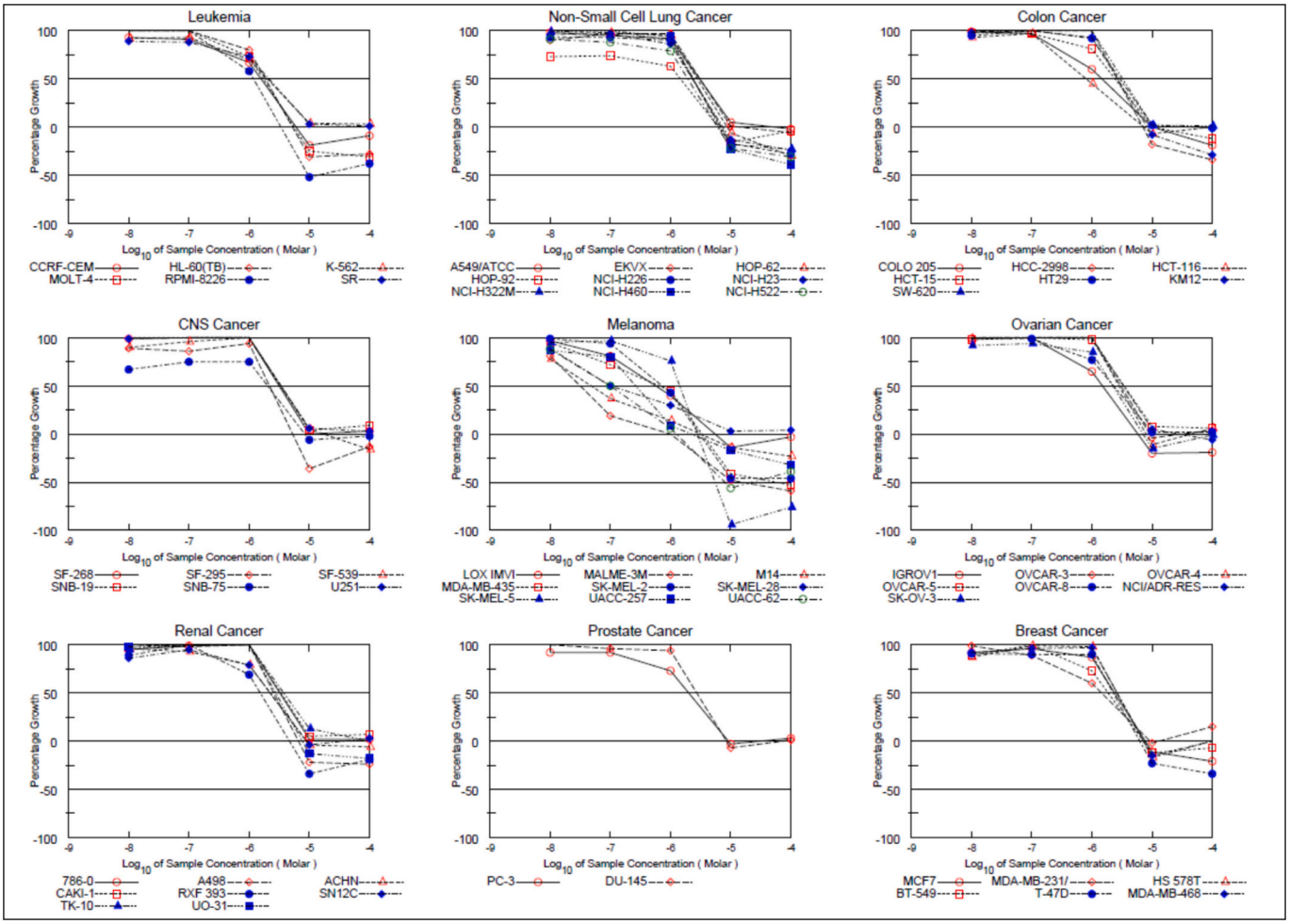

Fig. 6. *In vitro* cytotoxicity evaluation of **KS16** (**22g**) in five-point assay against NCI 60 human cancer cell lines.

Table 9
IC_{50} values (μM) of **22c**, **KS16**, vemurafenib **I**, sorafenib **VI** and **HM95574** against mutated BRAF ($BRAF^{V600E}$)-based human cancer cell lines.

Compound	IC_{50} values (μM)			
	Melanoma	Colon	Colorectal	
	A375	RKO	HCT116	HT29
22c	0.90 ± 0.11	4.51 ± 0.23	6.55 ± 0.34	10.27 ± 0.22
KS16	0.88 ± 0.07	3.97 ± 0.22	4.08 ± 0.38	7.47 ± 0.04
Vemurafenib **I**	0.88 ± 0.05	11.62 ± 2.44	ND[a]	7.87 ± 0.48
Sorafenib **VI**	5.25 ± 0.09	15.23 ± 2.62	ND	8.40 ± 0.55
HM95574	0.98 ± 0.04	2.87 ± 0.36	4.36 ± 0.79	ND

[a] **ND**, not determined.

optimal positioning of both binding motifs within their respective binding sites.

Given the limited size of the RAF selective back pocket, it was concluded that a phenyl ring is the optimal hydrophobic group to be accommodated within this region. Any modifications to this terminal group should be carefully considered to preserve potency. Small hydrophobic substitutions at positions 3 and 4 of the terminal phenyl ring maintain activity, whereas bulkier substitutions or polar groups are unfavorable. These larger modifications hinder accommodation within the restricted hydrophobic pocket, forcing the compound to adopt an alternative binding pose within the ATP active site, thereby affecting potency.

Notably, substitution at position 2 of the terminal phenyl ring, even with a small hydrophobic group, negatively impacts activity and affinity for the RAF selective back pocket. This is attributed to the disruption of the ring's planarity, which in turn affects binding to key hydrophobic amino acid residues within this iconic pocket. Furthermore, modifications to the distal phenyl ring at the solvent-exposed region significantly influence the activity of the designed compounds against $BRAF^{V600E}$. Incorporating a hydroxyl group (OH), which acts as both HBD and HBA, enhances potency by forming an HBD interaction with a key amino acid residue at the hinge region (Cys 532). In contrast, the methoxy (OMe) group, which functions solely as an HBA, does not provide the same binding pattern. However, the polar nature of the OH group increases the total polar surface area (TPSA) of the OH-bearing derivatives, which potentially affecting cell membrane permeability. Lastly, introducing a lipophilic fluorine atom (Series B) into the distal phenyl ring significantly enhances potency by enabling halogen interactions with key amino acid residues in the solvent-exposed area.

3.3.3. *In vitro cytotoxicity against sensitive and resistant cancer cell lines*

To evaluate the biological capability of **KS16** to inhibit the mutated BRAF-based cancer cells, it was tested against mutated BRAF ($BRAF^{V600E}$)-based human cancer cell lines (A375; melanoma cell line, and RKO; colon cancer cell line) using vemurafenib **I**, sorafenib **VI**, and **HM95574** as positive controls (Table 9) in ten-point assay. The results revealed that **KS16** showed the same IC_{50} value of that of vemurafenib against A375 cell line. In addition, **KS16** exhibited potent IC_{50} value

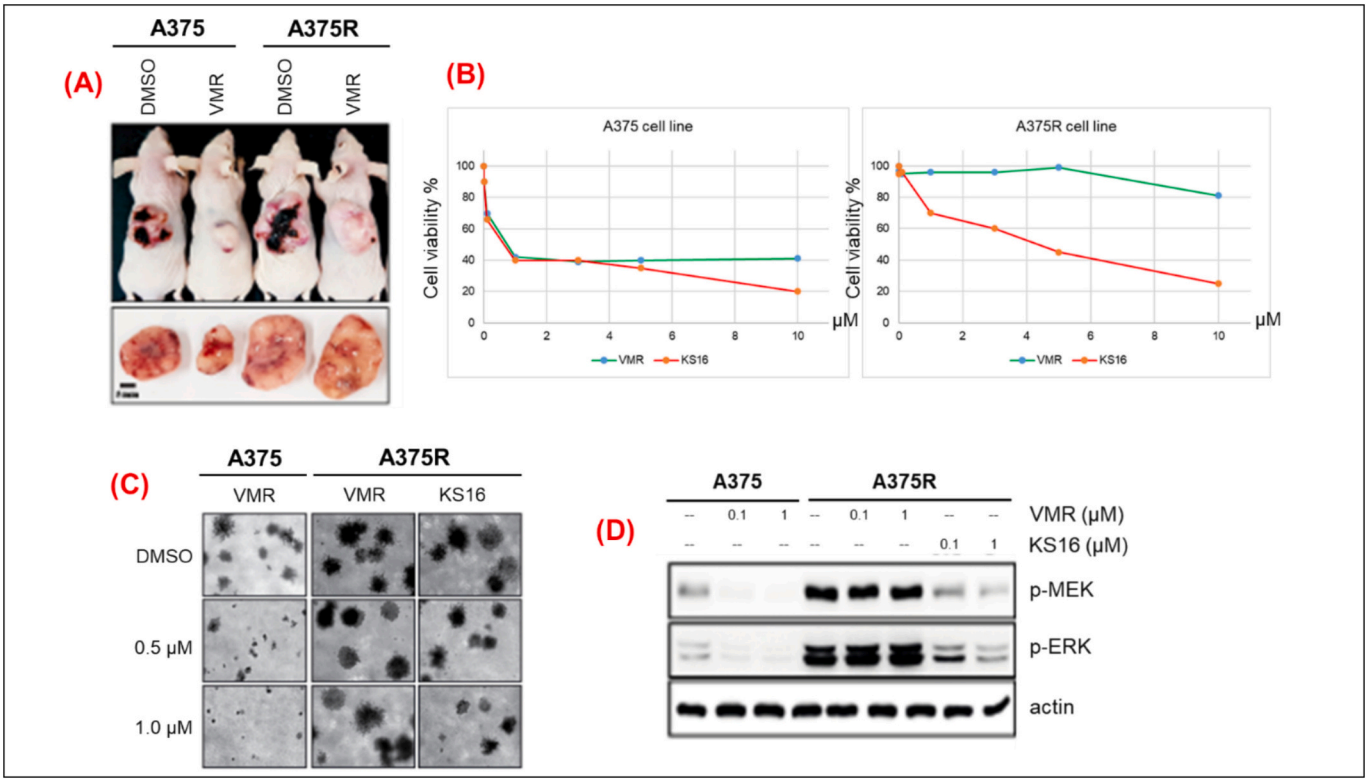

Fig. 7. **A**, the evaluation of vemurafenib resistance in A375R cells was confirmed at the cellular level. To observe the resistance effect in animal models, A375 cells and A375R cells were injected into Balb/C nude mice, followed by administration of vemurafenib **I**. As a result, in mice injected with A375 cells, tumor weight and size decreased with vemurafenib treatment, while no changes were observed in those injected with A375R cells. These results demonstrated that the established vemurafenib-resistant cells acquired strong resistance to vemurafenib in both cell culture and animal models, validating them as appropriate models for studying vemurafenib resistance; **B**, cells were seeded and incubated for 48 h in 10 % FBS/DMEM at 37 °C in 5 % CO_2 atmosphere. Then, the cells were treated with vemurafenib **I** and **KS16**. Cell viability was measured by MTT assay as described in experimental section. Data are represented as the means +/-S.D. as determined from triplicate experiment; **C**, colony formation inhibition was evaluated using vemurafenib **I** (in A375 and A375R cells) and **KS16** (in A375R cells). Treatment with vemurafenib resulted in a concentration-dependent decrease in colony size and number in A375 cells, but no change was observed in A375R cells. In A375R cells, colony formation was dose-dependently inhibited by **KS16**; **D**, the melanoma cell lines (A375 and A375R) were treated with 0.1 and 1 μM of **KS16** and vemurafenib **I**. After treatment of 24 h, cells were harvested and lysed. The levels of phosphorylated and total protein were determined by immunoblotting analysis using specific antibodies against MEK1/2 and ERK1/2, respectively.

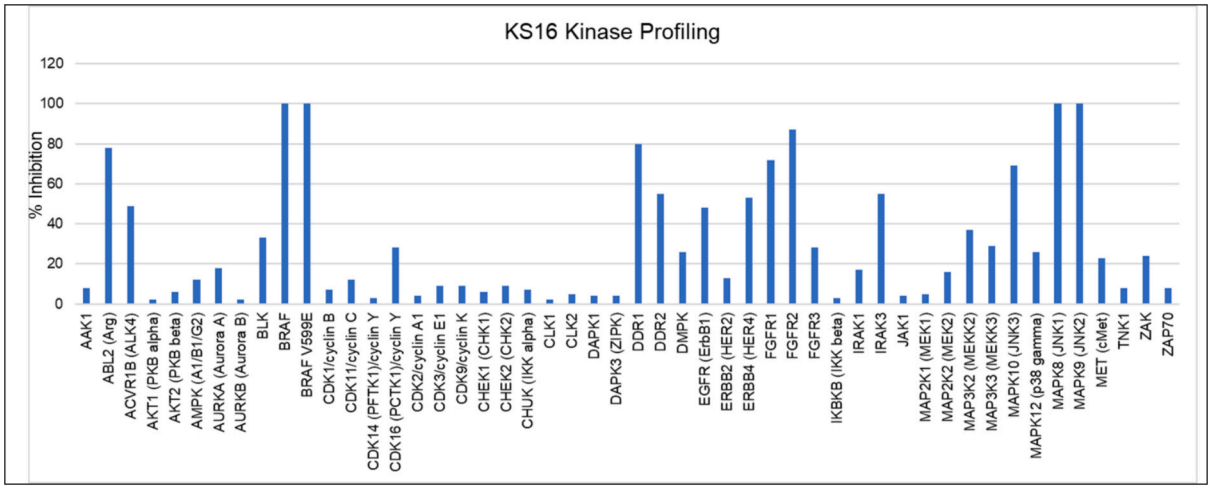

Fig. 8. The kinase profiling of **KS16** against different 50 protein kinases.

Table 10
IC_{50} values (nM) of **KS16** against panel of off-target kinase proteins.

Kinase	IC_{50} (nM)[a]	Selectivity index (SI)[b]
ABL2 (ARG)	598.0 ± 15.56	2300
DDR1	186.5 ± 13.44	717
FGFR1	230.0 ± 8.49	885
FGFR2	232.0 ± 14.14	892
JNK1	471.5 ± 57.28	1813
JNK2	20.4 ± 1.84	78
JNK3	3.2 ± 0.16	12

[a] The standard deviation values were calculated from duplicate assays.
[b] Selectivity index (SI) was calculated by dividing the off-target kinase IC_{50} values of **KS16** over the $BRAF^{V600E}$ IC_{50} value of **KS16** (0.26 nM).

Table 11
Tumor size (mm^3) and tumor weight (g) in BALB/c nude albino mice treated with **KS16** using vemurafenib **I** and **HM99574** as standards.

Compound	Group #	Dose (mg/kg)	Sample size	Tumor growth		% Survival
				Size (mm^3)	Weight (g)	
Saline	1	–	6	755	1.78	100
Vemurafenib **I**	2	50	6	65	0.25	100
HM95574	3	50	6	110	0.65	83.3
KS16	4	25	8	155	0.70	100
KS16	5	50	8	160	0.85	75

than that of sorafenib **VI** (reported to fail targeting $BRAF^{V600E}$-based melanoma cell lines) against A375. It is not surprising to observe discrepancies between the IC_{50} values of KS16 in the cell-based assay against A375 (0.88 μM) and the kinase inhibitory assay against $BRAF^{V600E}$ (0.26 nM). **KS16** and other derivatives designed in this study are classified as Type 1½ SMKIs, featuring extended chemical structures with high molecular weight that span both the hinge region and the selective back pocket of the ATP-binding site of the target protein ($BRAF^{V600E}$). These high-molecular-weight compounds suffer from poor cell permeability, which accounts for these discrepancies. Moreover, **KS16** showed potent IC_{50} value than that of both vemurafenib **I** and sorafenib **VI** against human colon cancer cell line (RKO). The results suggested that **KS16** will be a promising drug candidate for patients who suffer from mutated BRAF-based melanoma and colon cancers as it showed better biological profile that that of vemurafenib **I**.

To explore the effect of **KS16** on resistant cell lines, our main objectives in this current study, it was tested against drug-resistant model of A375 human melanoma cell line (A375R) using vemurafenib **I** as negative standard (Fig. 7). **KS16** showed promising activity against A375R cell lines and can inhibit the growth of these cancer cells in contrast to vemurafenib **I** which failed to exhibit any significant inhibition to the drug-resistant human melanoma cell line model (A375R, Fig. 7).

3.3.4. *In vitro kinase panel assay (kinome profiling)*

Additionally, **KS16** was tested biologically against broad panel of protein kinases (50 kinases) in one-point assay (10 μM) to identify its kinase inhibition profile. The tested kinases were selected among the human kinome tree which have similarities with RAF kinases (**Table S1** and Fig. 8). The results revealed that **KS16** showed high selectivity index against RAF kinases over the other tested kinases. Additionally, **KS16** showed moderate inhibition (75–90 %) to four kinases (ABL2/ARG, DDR1, FGFR1, and FGFR2). Interestingly, **KS16** exhibit remarkable inhibition to JNK isoforms. Recent biological studies have observed a high level of JNK pathway activation in some human BRAF inhibitor-resistant melanoma cell lines relative to their BRAF inhibitor-sensitive isogenic counterparts [63,64]. To confirm the selectivity profile of **KS16**, which reflects its minimal off-target effects, we conducted a biochemical assay to determine its IC_{50} values against the following kinases: ABL2/ARG, DDR1, FGFR1, FGFR2, JNK1, JNK2, and JNK3 using the same experimental protocol as in the *in vitro* kinase inhibitory assay. Both IC_{50} values and the selectivity index is described in Table 10. The results revealed that **KS16** exhibited a high selectivity index (SI > 500 for ABL2/ARG, DDR1, FGFR1, FGFR2, and JNK1, and SI > 50 for JNK2), allowing for selective BRAF kinase inhibition in a dose-dependent manner, thereby minimizing off-target effects. Although **KS16** showed an SI of 12 for JNK3 (predominantly expressed in the brain), it is unlikely to exhibit significant off-target effects on the centrally occurring JNK3 kinase, as **KS16** showed high molecular weight (542.58 Da), high tPSA (118.75 Å), and cLogP of 4.79 to penetrate the blood-brain barrier (BBB). Therefore, it is suggested that **KS16** can tackle the drug-resistant melanoma through different pathways, particularly JNK2 kinase, to overcome any acquired resistance with minimal off-target effect.

3.3.5. *In vivo antitumor evaluation*

KS16 was evaluated for its *in vivo* antiproliferative efficacy in A375 melanoma xenograft mouse model: BALB/c nude albino mice using vemurafenib **I** and **HM95574** as positive controls and saline as negative control. The compound was evaluated at two different doses (25 and 50 mg/kg in groups 4 and 5, respectively). That doses were well tolerated by the animals as per the *in vivo* toxicity experiment (% survival 100 and 75 % for group 4 and 5, respectively). The tumor volume (mm^3) and

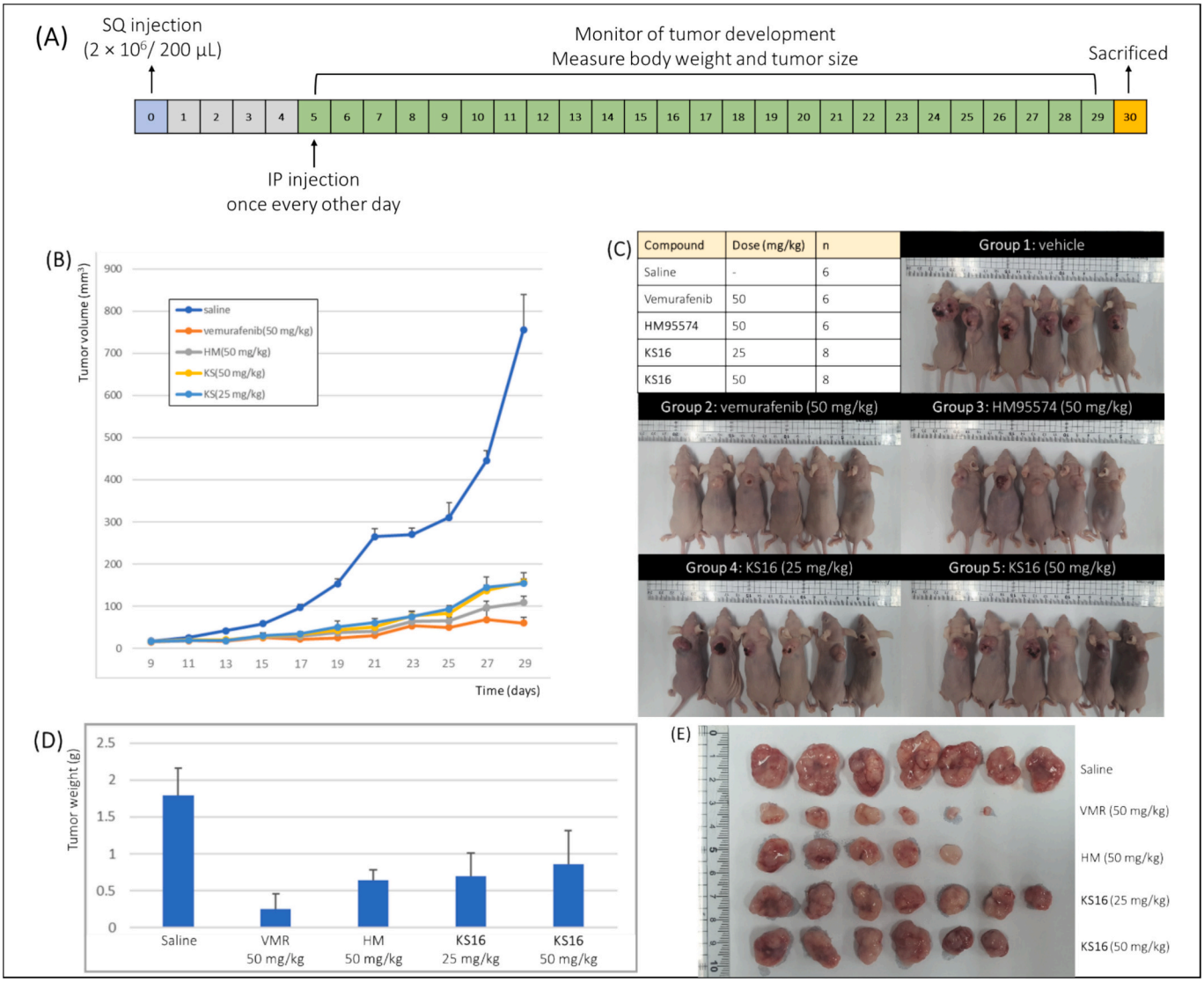

Fig. 9. *In vivo* antiproliferative assay of **KS16** in A375 melanoma xenograft mouse model (BALB/c nude albino mice). A, the time frame of *in vivo* assay including sample injection and tumor size monitoring; B, the progression of tumor (volume) over time across the *in vivo* assay timeline using saline as negative control, and vemurafenib **I** and **HM95574** as positive control; C, the tumor progression in animal model across the five groups of *in vivo* assay (six mice/group); D, the difference between the progressed tumor (weight) among the assay 5 groups; E, the isolated tumor from the tested model showing the effect of the **KS16** compared to the negative control (saline) and positive control (vemurafenib **I** and **HM95574**).

weight (g) were measured to identify the antitumor activity of the compound of interest (**KS16**). The results were described in Table 11 and Fig. 9. The *in vivo* results revealed that **KS16** showed antiproliferative activity in both doses (25 and 50 mg/kg) compared to the control group (group 1: saline). Unexpectedly, a larger tumor size and weight were obtained at 50 mg/kg compared to 25 mg/kg. This discrepancy was suggested to arise from a nonlinear dose-response, where higher doses do not always lead to greater efficacy due to potential target saturation or the activation of compensatory survival pathways. Additionally, adaptation within the tumor microenvironment may occur, as the higher dose can induce hypoxia, triggering angiogenesis and possibly promoting tumor growth instead of suppression. Potential systemic toxicity may contribute to these unexpected findings, as higher doses can alter drug metabolism or immune responses, inadvertently reducing overall anti-tumor effects. Despite this anomaly, other dosage groups showed consistent tumor suppression. Although **KS16** showed the same potent activity of vemurafenib **I** in *in vitro* antiproliferative evaluation against A375 melanoma cell lines (Table 11), but it exhibited lower antiproliferative activity compared to the standards used in this *in vivo* study (vemurafenib **I** and **HM99574**). It was suggested that the compound was affected by metabolism and the clearance in BALB/c nude albino mice that affected its half lifetime and the pharmacological response in the *in vivo* study.

Table 12
IC_{50} values (µM) of selected compounds (**22b**, **22c**, and **KS16**) over normal skin fibroblast cell line (BJ1).

Compound	BJ1 IC_{50}	Selectivity index (SI)[a]
22b	41.55 ± 2.12	ND[b]
22c	63.0 ± 1.52	ND
KS16	61.1 ± 3.15	70

[a] Selectivity index (SI) was calculated by dividing the BJ1 normal skin fibroblast cell line IC_{50} value over the A375 melanoma cell line IC_{50} value.

3.3.6. Normal cell cytotoxicity assay

To evaluate the toxicity of the synthesized compound (series B) over normal cell lines, three compounds (**22b**, **22c**, and **KS16**) were selected

Table 13
In vitro biological assay of **KS16**, vemurafenib **I** and **HM95574** against different MAPK-signalling pathway proteins.

Compound	K-Ras	H-Ras	$BRAF^{WT}$	CRAF
	% Inhibition		IC_{50} values (nM)	
KS16	76 %	69 %	0.96	0.38
Vemurafenib **I**	40 %	16 %	>10	>10
HM95574	2 %	<1 %	–	–

to be assessed against normal skin fibroblast cell line (BJ1) to identify their IC_{50} values (Table 12). The selectivity index of **KS16** (most potent compound) was calculated taking in consideration the IC_{50} against A375 melanoma cell line. All tested compounds exhibited a high IC_{50} over BJ1 cell lines, indicating a substantial therapeutic index for these compounds. Comparing the activity of **KS16** over both melanoma cell lines (0.88 μM) and the BJ1 cell line (61.10 μM) revealed a 70-fold higher selectivity toward melanoma than normal cells.

3.3.7. Activity over K-Ras and H-Ras

To explore the mode of action of **KS16** over the MAPK signalling cascade key elements, **KS16** was tested to identify its ability to inhibit the phosphorylation of both K-Ras and H-Ras proteins using vemurafenib **I** and **HM95574** as positive and negative controls, respectively (Table 13 and Fig. 10). **KS16** exhibited significant inhibition profiles against both K-Ras and H-Ras compared to that of vemurafenib **I** and **HM95574**. These results afford additional capacity of **KS16** to hit different key spots within MAPK signalling pathway than that of vemurafenib **I**. Moreover, **KS16** was tested against other RAF isoforms to evaluate its ability to block the CRAF-based resistance using vemurafenib **I** as standard (Table 13). The results revealed that the **KS16** showed a significant IC_{50} value against CRAF kinase enzyme than that of vemurafenib. It is suggested that **KS16** can block this resistance pathway affording an additional arm to stop the drug-resistant melanoma.

3.3.8. Activity over hERG

The drug-candidate safety profile of **KS16** was emphasized in this current project as there is a number of drugs that have been withdrawn from late-stage clinical trials due to their cardiotoxic effects. The human ether-a-go-go related gene (hERG) encodes the inward rectifying voltage gated potassium channel in the heart (I_{Kr}) which is involved in cardiac repolarization. Blockade and inhibition of the hERG current causes QT interval prolongation resulting in potentially fatal ventricular tachyarrhythmia (Torsade de Pointes) that can lead to cardiac arrhythmia, which has become a major concern in drug discovery and development [65]. Therefore, the drug safety evaluation during non-clinical drug development is important in any drug discovery project. **KS16** was tested against hERG using **E4031** (IC_{50} = 0.025 μM) as positive control to set up the hERG channel binding assay (Table 14 and Fig. 11). The results revealed that **KS16** showed relatively weak binding to hERG (% inh = 64 %) at 10 μM compared to that of the potent positive control (**E4031**, % inh = 97 %) at the same molar concentration of **KS16**. The hERG safety assay revealed that **KS16** can be considered a promising drug-like candidate with limited cardiotoxicity profile.

3.3.9. In vivo pharmacokinetic analysis

The *in vivo* PK profile of **KS16** with additional two selected compounds among the potent series (series B; **22b** and **22c**) were investigated to evaluate the drug-like properties of these candidates (Table 15 and Figs. S36–54). The tested compounds were tested in male mice (IV, 5 mg/Kg and PO, 10 mg/kg) to evaluate the plasma concentration curve and to measure the pharmacokinetic parameters for both IV and PO administration. The results revealed that **KS16** showed better pharmacokinetic profile than that of our previously developed compound **VII**. **KS16** showed half-life of 5.46 h and 2.09 h following IV and PO administration, respectively (compared to compound **VII**; 1.72 h (IV) and 3.35 h (PO). However, it showed high clearance compared to that of compound **VII** (3.04 and 2.07 L/h/kg, respectively).

3.3.10. Microsomal stability

This experiment evaluates how extensively drugs are metabolized in the liver, the main organ responsible for drug metabolism, by using liver microsomes. This helps predict the stability of **KS16** within the body. Metabolic stability is a crucial parameter for drug candidates as it influences pharmacokinetic parameters such as clearance, half-life, and oral bioavailability. The human metabolic stability of **KS16** was expressed as the percentage activity relative to the control using verapamil as standard (Table 16). The results revealed that the compound (**KS16**) is more stable (70.9 %), compared to that of veramapil (16 %), with half-life 30–60 min.

3.3.11. CYP450 inhibition assay

This assay measures the extent of inhibition of CYP enzymes, the major drug-metabolizing enzymes in the human body, to predict the possible drug interactions. It serves as foundational data for ensuring the safety and efficacy evaluation of compounds within the Drug Discovery phase. Two compounds, among series B, were selected to be evaluated in this current assay (**22c** and **KS16**). The inhibition was expressed as a percentage of activity over five isoforms of CY450 (CYP1A2, CYP2C9, CYP2C19, CYP2D6, and CYP3A4) relative to the control using

Table 14
hERG channel binding assay results (% inh) of **KS16** and **E4031** as positive control.

Compound	% Inh
KS16	64 %
E4031	97 %

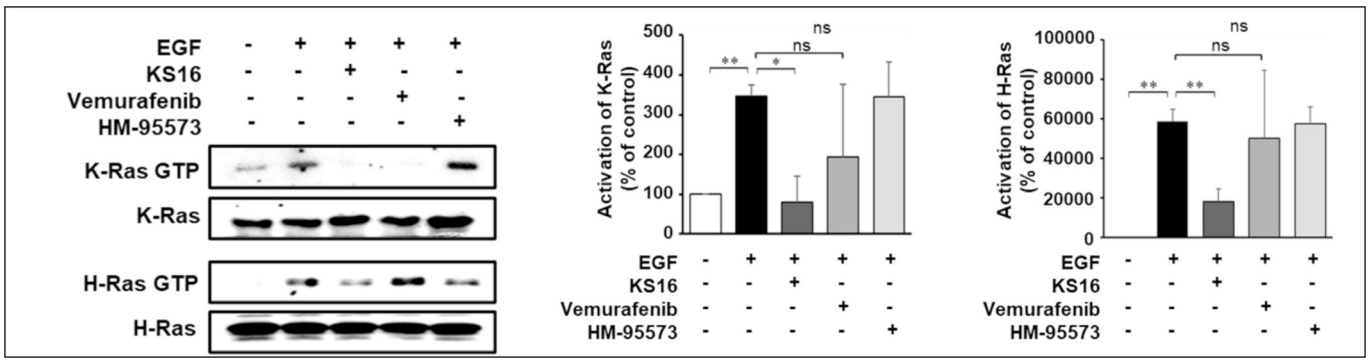

Fig. 10. Immunoblotting analysis of **KS16** in melanoma cell line using vemurafenib **I** (positive control and **HM95574** (negative control). **KS16** showed significant inhibition of phosphorylation of both K-Ras and H-Ras compared to that of used controls.

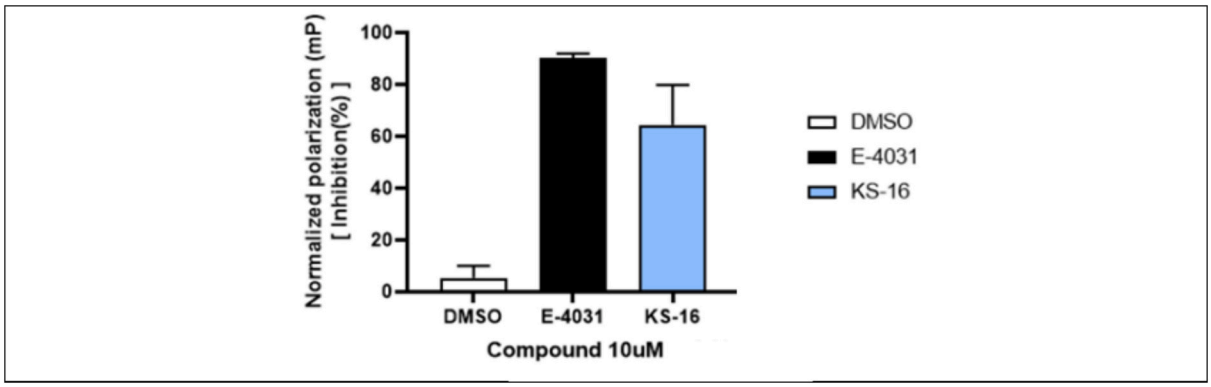

Fig. 11. hERG channel binding assay of **KS16** using DMSO and **E4031** as negative and positive control, respectively at 10 μM concentration. **KS16** showed relatively weak inhibition to hERG compared to that of positive control (**E4031**).

Table 15
In vivo pharmacokinetic parameters of **22b**, **22c**, and **KS16** in male mice.

Parameters	IV			PO		
	22b	22c	KS16	22b	22c	KS16
T_{max} (h)	NA	NA	NA	0.25 ± 0	0.25 ± 0	0.33 ± 0.14
C_{max} (μg/mL)	NA	NA	NA	0.39 ± 0.06	0.55 ± 0.15	0.7 ± 0.49
$T_{1/2}$ (h)	3.41 ± 1.94	2.27 ± 1.34	5.46 ± 5.26	3.25 ± 1.5	0.89 ± 0.15	2.09 ± 1.34
AUC_{last} (μg.h/mL)	0.49 ± 0.21	1.35 ± 0.04	1.72 ± 0.52	0.24 ± 0.02	0.4 ± 0.18	0.37 ± 0.19
AUC_{∞} (μg.h/mL)	0.51 ± 0.2	1.35 ± 0.05	1.73 ± 0.51	0.24 ± 0.02	0.4 ± 0.18	0.37 ± 0.19
CL (L/h/kg)	10.69 ± 3.4	3.71 ± 0.13	3.04 ± 0.78	NA	NA	NA
V_{ss} (L/kg)	34.0 ± 43.8	1.65 ± 0.84	2.23 ± 1.74	NA	NA	NA
MRT_{last} (h)	1.67 ± 1.96	0.37 ± 0.17	0.42 ± 0.3	1.37 ± 0.75	0.99 ± 0.35	0.94 ± 0.63
MRT_{∞} (h)	2.72 ± 3.31	0.44 ± 0.23	0.65 ± 0.46	1.59 ± 1.03	1.03 ± 0.34	1.12 ± 0.81
F_t (%)	NA	NA	NA	24.45 %	14.75 %	10.76 %

T_{max}, time for C_{max}; **C_{max}**, maximum plasma concentration; **$T_{1/2}$**, terminal half-life; **AUC_{last}**, areas under the plasma concentration-time curve from time zero to time of last measurable concentration; **AUC_{∞}**, areas under the plasma concentration-time curve from time zero to time infinity; **CL**, total clearance from plasma; **V_{ss}**, steady-state volume of distribution; **MRT_{last}**, mean residence time at last measurable concentration; **MRT_{∞}**, mean residence time explorated to infinity; **F_t**, bioavailability (AUC_{PO}/AUC_{IV}) × 100; **IV**, intravenous (5 mg/kg); **PO**, oral (10 mg/kg); **NA**, not applicable.

Table 16
Human liver microsomal stability (% Remaining during 30 min).

Compound	Human (%)
KS16	70.9 %
Verapamil	16.0 %

ketoconazole as standard (reported CYP3A4 inhibitor; IC_{50} 0.1 μM, Table 17). The results revealed that both of tested compounds showed weak inhibition to CY450 isoforms compared to that of ketoconazole. Additionally, **KS16** (the most active compound among the synthesized series A and B) showed minimal inhibition compared to **22c** across the tested CY450 isoforms. The results revealed that **KS16** is a promising candidate that will show minimal drug interaction in its pharmacodynamic profile.

4. Conclusion

In this study, we successfully designed and synthesized first-in-class imidazothiazole-based derivatives as $BRAF^{V600E}$ inhibitors, targeting drug-resistant melanoma. Two distinct series (A: pyridine-based, B: pyrimidine-based) were developed through an optimized and sustainable synthetic route. Both series exhibited a binding mode similar to vemurafenib **I** (FDA-approved $BRAF^{V600E}$ inhibitor) but with enhanced hydrophobic interactions within the RAF selective back pocket. In contrast to vemurafenib **I** that possess small-sized terminal propyl group which failed to perfectly fit into this iconic pocket.

Among the synthesized compounds, **KS16** (series B) emerged as the most potent candidate, demonstrating nanomolar inhibition of $BRAF^{V600E}$ kinase (0.26 nM) and selective cytotoxicity against NCI melanoma cell lines (mean $GI_{50} = 0.43$ μM). Molecular docking revealed a key halogen interaction at solvent-exposed area with Gly 534, contributing to its enhanced binding affinity. **KS16** exhibited superior activity against drug-resistant melanoma cells (A375R), selective kinase inhibition, and favorable *in vivo* anticancer efficacy in melanoma-bearing models. Additionally, **KS16** showed a promising pharmacokinetic profile, improved metabolic stability, and minimal CYP450 inhibition, indicating low potential for drug-drug interactions.

These findings highlight **KS16** as a promising lead compound for drug-resistant melanoma. Based on predictive *in silico* studies using a rigid molecular docking protocol to generate our hypothesis, further validation through obtaining cocrystal structure of BRAF kinase and the selected developed compound (**KS16**) is needed to validate the binding mode, particularly the key role of the highlighted back pocket, and confirm the proposed the proposed structure activity relationship (SAR).

Table 17
CYP enzyme inhibition data (%) of **22c** and **KS16** using ketoconazole as standard.

Compound	% inhibition				
	CYP1A2	CYP2C9	CYP2C19	CYP2D6	CYP3A4
22c	35.1 %	34.7 %	8.6 %	22.7 %	12.3 %
KS16	27.2 %	8.9 %	11.9 %	23.6 %	6.7 %
Ketoconazole[a]	> 100 %	> 100 %	> 100 %	> 100 %	27.2 %

[a] Reported CYP3A4 inhibitor (IC_{50} 0.1 μM).

Further structural optimization and mechanistic studies are underway to refine its drug-like properties and explore its therapeutic potential in resistant melanoma models.

Abbreviations

Ala	alanine
Asp	aspartic acid
ATP	adenosine triphosphate
CDM	dichloromethane
CNS	central nervous system
CYP	cytochrome P450
Cys	cysteine
DIPEA	*N*,*N*-diisopropylethylamine
DMF	dimethylformamide
DMSO	dimethyl sulfoxide
ERK	extracellular signal-regulated kinases
Et_3N	triethylamine
EtOAc	ethyl acetate
FDA	Food and Drug Administration
GI_{50}	growth inhibition 50 %
Gly	glycine
HBAs	hydrogen bond acceptors
HBDs	hydrogen bond donors
hERG	human ether-a-go-go
HPLC	High Pressure Liquid Chromatography
HRMS	high resolution mass spectroscopy IC_{50}, half maximal inhibitory concentration
Ile	isoleucine
Inh%	inhibition%
IV	intravenous
JNK	c-jun *N*-terminal kinase
KIs	kinase inhibitors
Leu	leucine
LiHMDS	lithium *bis*(trimethylsilyl)amide
MAPK	mitogen-activated protein kinase
MeCN	acetonitrile
MEK	mitogen-activated protein kinase kinase
MeOH	methanol
NBS	*N*-bromosuccinamide
NCI	National Cancer Institute
PDB	protein data bank
Phe	phenyl alanine
PK	protein kinase
PO	oral administration
RAF	rapidly accelerated fibrosarcoma
RAS	rat sarcoma virus
RTKs	receptor tyrosine kinases
SNAr	nucleophilic aromatic substitution
THF	tetrahydrofuran
Thr	threonine
TPSA	topological polar surface area
Trp	tryptophan
Tyr	tyrosine

CRediT authorship contribution statement

Usama Ammar: Writing – review & editing, Writing – original draft, Supervision, Software, Resources, Methodology, Funding acquisition, Data curation, Conceptualization. **Mahmoud Gamal El-Din:** Visualization, Methodology, Formal analysis, Data curation, Conceptualization. **Mohammed Abdel-Maksoud:** Writing – review & editing, Visualization, Validation, Supervision, Methodology, Investigation, Data curation, Conceptualization. **Eslam Ali:** Writing – review & editing, Validation, Methodology, Investigation, Formal analysis. **Mohammed I. El-Gamal:** Writing – review & editing, Validation, Resources, Funding acquisition, Data curation. **Zeyad Mahmoud:** Visualization, Methodology, Investigation. **Sunjoo Ahn:** Visualization, Validation, Resources, Investigation, Formal analysis, Data curation. **Nhung Hong Nguyen:** Visualization, Validation, Resources, Investigation, Formal analysis, Data curation. **Eunkyoung Kim:** Visualization, Validation, Resources, Investigation, Formal analysis, Data curation. **Park Su Jun:** Visualization, Validation, Software, Resources, Investigation, Formal analysis, Data curation. **Kim Young Deug:** Visualization, Validation, Resources, Methodology, Investigation, Formal analysis, Data curation. **Hong Seok Choi:** Visualization, Validation, Resources, Methodology, Investigation, Formal analysis, Data curation. **Kwan Hyi Lee:** Visualization, Validation, Resources, Methodology, Investigation, Formal analysis, Data curation. **Gahyeon Choi:** Visualization, Validation, Resources, Methodology, Investigation, Formal analysis, Data curation. **Chang-Hyun Oh:** Visualization, Validation, Resources, Methodology, Investigation, Formal analysis, Data curation.

Funding

This work was supported by Korea Institute of Science and Technology, South Korea (projects Nos 2E32311 and 2E32351); Edinburgh Napier University, United Kingdom (project No 2988878); and University of Sharjah, United Arab Emirates (Project No. 24011101106).

Declaration of competing interest

The authors declare that they have no known competing financial interests or personal relationships that could have appeared to influence the work reported in this paper.

Acknowledgments

We would like to thank Korea Institute of Science and Technology (KIST) for their financial support (projects Nos 2E32311 and 2E32351). We express our sincere appreciation to Edinburgh Napier University (project No 2988878) for supporting and contributing to this work. We sincerely thank University of Sharjah, United Arab Emirates (Project No. 24011101106) for its support and valuable contributions to this work. The authors are grateful to the National Cancer Institute (NCI), Bethesda, Maryland, USA, for testing the antiproliferative activity of the target compounds against the NCI-60 cancer cell line panel of nine different cancer types.

Appendix A. Supplementary data

The data including Kinome profiling of **KS16** (Table S1), NCI data summarizing the growth inhibition values of the target compounds over NCI-60 cell line panel (Figs. S1–35), PK profiling analysis of target compounds **22b**, **22c**, and **KS16** (Figs. S36–54), NMR spectra and characterization of synthesized compounds (Figs. S55–128), HPLC traces showing the purity of tested compounds (Figs. S129–142), and binding mode of compounds **11b**, **112b**, **12h**, and **22g** (**KS16**) within the ATP active site of $BRAF^{V600E}$ (3OG7) are provided in the supplementary file. Supplementary data to this article can be found online at https://doi.org/10.1016/j.ijbiomac.2025.145699.

Data availability

Data will be made available on request.

References

[1] J. Ferlay, I. Soerjomataram, R. Dikshit, S. Eser, C. Mathers, M. Rebelo, D.M. Parkin, D. Forman, F. Bray, Cancer incidence and mortality worldwide: sources, methods and major patterns in GLOBOCAN 2012, Int. J. Cancer 136 (5) (2015) E359–E386.

[2] H.-L. Li, M.-M. Su, Y.-J. Xu, C. Xu, Y.-S. Yang, H.-L. Zhu, Design and biological evaluation of novel triaryl pyrazoline derivatives with dioxane moiety for selective BRAFV600E inhibition, Eur. J. Med. Chem. 155 (2018) 725–735.
[3] Y. Wang, S. Wan, Z. Li, Y. Fu, G. Wang, J. Zhang, X. Wu, Design, synthesis, biological evaluation and molecular modeling of novel 1H-pyrazolo [3, 4-d] pyrimidine derivatives as BRAFV600E and VEGFR-2 dual inhibitors, Eur. J. Med. Chem. 155 (2018) 210–228.
[4] Y. Sun, W.-Z. Liu, T. Liu, X. Feng, N. Yang, H.-F. Zhou, Signaling pathway of MAPK/ERK in cell proliferation, differentiation, migration, senescence and apoptosis, J. Recept. Signal Transduction 35 (6) (2015) 600–604.
[5] L.H. Al-Wahaibi, A.M. Gouda, O.F. Abou-Ghadir, O.I. Salem, A.T. Ali, H. S. Farghaly, M.H. Abdelrahman, L. Trembleau, H.H. Abdu-Allah, B.G. Youssif, Design and synthesis of novel 2, 3-dihydropyrazino [1, 2-a] indole-1, 4-dione derivatives as antiproliferative EGFR and BRAFV600E dual inhibitors, Bioorg. Chem. 104 (2020) 104260.
[6] K.S. Bhullar, N.O. Lagarón, E.M. McGowan, I. Parmar, A. Jha, B.P. Hubbard, H. V. Rupasinghe, Kinase-targeted cancer therapies: progress, challenges and future directions, Mol. Cancer 17 (2018) 1–20.
[7] P. Cohen, Protein kinases—the major drug targets of the twenty-first century? Nat. Rev. Drug Discov. 1 (4) (2002) 309–315.
[8] D. Sun, Y. Zhao, S. Zhang, L. Zhang, B. Liu, L. Ouyang, Dual-target kinase drug design: current strategies and future directions in cancer therapy, Eur. J. Med. Chem. 188 (2020) 112025.
[9] H.T. Abdel-Mohsen, M.A. Omar, A.M. El Kerdawy, A.E. Mahmoud, M.M. Ali, H.I. El Diwani, Novel potent substituted 4-amino-2-thiopyrimidines as dual VEGFR-2 and BRAF kinase inhibitors, Eur. J. Med. Chem. 179 (2019) 707–722.
[10] J. Brognard, T. Hunter, Protein kinase signaling networks in cancer, Curr. Opin. Genet. Dev. 21 (1) (2011) 4–11.
[11] M.A. Lemmon, J. Schlessinger, Cell signaling by receptor tyrosine kinases, Cell 141 (7) (2010) 1117–1134.
[12] K. Parang, G. Sun, Protein kinase inhibitors drug discovery, in: Drug Discovery Handbook, 2005, pp. 1191–1257.
[13] M. Pearson, C. García-Echeverría, D. Fabbro, Protein Tyrosine Kinases as Targets for cancer and Other Indications, Protein Tyrosine Kinases: From Inhibitors to Useful Drugs, Springer, 2006, pp. 1–29.
[14] A.A. Aly, E.M. El-Sheref, M.E. Bakheet, M.A. Mourad, S. Bräse, M.A. Ibrahim, M. Nieger, B.K. Garvalov, K.N. Dalby, T.S. Kaoud, Design, synthesis and biological evaluation of fused naphthofuro [3, 2-c] quinoline-6, 7, 12-triones and pyrano [3, 2-c] quinoline-6, 7, 8, 13-tetraones derivatives as ERK inhibitors with efficacy in BRAF-mutant melanoma, Bioorg. Chem. 82 (2019) 290–305.
[15] J.F. Blake, M. Burkard, J. Chan, H. Chen, K.-J. Chou, D. Diaz, D.A. Dudley, J. J. Gaudino, S.E. Gould, J. Grina, Discovery of (S)-1-(1-(4-Chloro-3-Fluorophenyl)-2-Hydroxyethyl)-4-(2-((1-Methyl-1 H-Pyrazol-5-Yl) Amino) Pyrimidin-4-yl) Pyridin-2 (1 H)-one (GDC-0994), An Extracellular Signal-Regulated Kinase 1/2 (ERK1/2) Inhibitor in Early Clinical Development, ACS Publications, 2016.
[16] R.J. Sullivan, J.R. Infante, F. Janku, D.J.L. Wong, J.A. Sosman, V. Keedy, M. R. Patel, G.I. Shapiro, J.W. Mier, A.W. Tolcher, First-in-class ERK1/2 inhibitor ulixertinib (BVD-523) in patients with MAPK mutant advanced solid tumors: results of a phase I dose-escalation and expansion study, Cancer Discov. 8 (2) (2018) 184–195.
[17] M.W. Hoorens, M.E. Ourailidou, T. Rodat, P.E. van der Wouden, P. Kobauri, M. Kriegs, C. Peifer, B.L. Feringa, F.J. Dekker, W. Szymanski, Light-controlled inhibition of BRAFV600E kinase, Eur. J. Med. Chem. 179 (2019) 133–146.
[18] L.E. Campos, F.M. Garibotto, E. Angelina, J. Kos, T. Tomašič, N. Zidar, D. Kikelj, T. Gonec, P. Marvanova, P. Mokry, Searching new structural scaffolds for BRAF inhibitors. An integrative study using theoretical and experimental techniques, Bioorganic Chemistry 91 (2019) 103125.
[19] M. Dankner, A.A. Rose, S. Rajkumar, P.M. Siegel, I.R. Watson, Classifying BRAF alterations in cancer: new rational therapeutic strategies for actionable mutations, Oncogene 37 (24) (2018) 3183–3199.
[20] P.T. Wan, M.J. Garnett, S.M. Roe, S. Lee, D. Niculescu-Duvaz, V.M. Good, C. M. Jones, C.J. Marshall, C.J. Springer, D. Barford, Mechanism of activation of the RAF-ERK signaling pathway by oncogenic mutations of B-RAF, Cell 116 (6) (2004) 855–867.
[21] M.W. Rowbottom, R. Faraoni, Q. Chao, B.T. Campbell, A.G. Lai, E. Setti, M. Ezawa, K.G. Sprankle, S. Abraham, L. Tran, Identification of 1-(3-(6, 7-dimethoxyquinazolin-4-yloxy) phenyl)-3-(5-(1, 1, 1-trifluoro-2-methylpropan-2-yl) isoxazol-3-yl) urea hydrochloride (CEP-32496), a highly potent and orally efficacious inhibitor of V-RAF murine sarcoma viral oncogene homologue B1 (BRAF) V600E, J. Med. Chem. 55 (3) (2012) 1082–1105.
[22] H. Davies, G.R. Bignell, C. Cox, P. Stephens, S. Edkins, S. Clegg, J. Teague, H. Woffendin, M.J. Garnett, W. Bottomley, Mutations of the BRAF gene in human cancer, Nature 417 (6892) (2002) 949–954.
[23] M. Holderfield, M.M. Deuker, F. McCormick, M. McMahon, Targeting RAF kinases for cancer therapy: BRAF-mutated melanoma and beyond, Nat. Rev. Cancer 14 (7) (2014) 455–467.
[24] P.B. Chapman, A. Hauschild, C. Robert, J.B. Haanen, P. Ascierto, J. Larkin, R. Dummer, C. Garbe, A. Testori, M. Maio, Improved survival with vemurafenib in melanoma with BRAF V600E mutation, New England Journal of Medicine 364 (26) (2011) 2507–2516.
[25] A. Hauschild, J.-J. Grob, L.V. Demidov, T. Jouary, R. Gutzmer, M. Millward, P. Rutkowski, C.U. Blank, W.H. Miller, E. Kaempgen, Dabrafenib in BRAF-mutated metastatic melanoma: a multicentre, open-label, phase 3 randomised controlled trial, Lancet 380 (9839) (2012) 358–365.
[26] J.-P. Delord, C. Robert, M. Nyakas, G.A. McArthur, R. Kudchakar, A. Mahipal, Y. Yamada, R. Sullivan, A. Arance, R.F. Kefford, Phase I dose-escalation and-expansion study of the BRAF inhibitor encorafenib (LGX818) in metastatic BRAF-mutant melanoma, Clin. Cancer Res. 23 (18) (2017) 5339–5348.
[27] J.R. Henry, M.D. Kaufman, S.-B. Peng, Y.M. Ahn, T.M. Caldwell, L. Vogeti, H. Telikepalli, W.-P. Lu, M.M. Hood, T.J. Rutkoski, Discovery of 1-(3, 3-Dimethylbutyl)-3-(2-Fluoro-4-Methyl-5-(7-Methyl-2-(Methylamino) Pyrido [2, 3-d] Pyrimidin-6-Yl) Phenyl) Urea (LY3009120) as a pan-RAF Inhibitor with Minimal Paradoxical Activation and Activity against BRAF or RAS Mutant Tumor Cells, ACS Publications, 2015.
[28] K.T. Flaherty, I. Puzanov, K.B. Kim, A. Ribas, G.A. McArthur, J.A. Sosman, P. J. O'Dwyer, R.J. Lee, J.F. Grippo, K. Nolop, Inhibition of mutated, activated BRAF in metastatic melanoma, N. Engl. J. Med. 363 (9) (2010) 809–819.
[29] M. Griffin, D. Scotto, D.H. Josephs, S. Mele, S. Crescioli, H.J. Bax, G. Pellizzari, M. D. Wynne, M. Nakamura, R.M. Hoffmann, BRAF inhibitors: resistance and the promise of combination treatments for melanoma, Oncotarget 8 (44) (2017) 78174.
[30] C. Montagut, S.V. Sharma, T. Shioda, U. McDermott, M. Ulman, L.E. Ulkus, D. Dias-Santagata, H. Stubbs, D.Y. Lee, A. Singh, Elevated CRAF as a potential mechanism of acquired resistance to BRAF inhibition in melanoma, Cancer Res. 68 (12) (2008) 4853–4861.
[31] S.J. Heidorn, C. Milagre, S. Whittaker, A. Nourry, I. Niculescu-Duvas, N. Dhomen, J. Hussain, J.S. Reis-Filho, C.J. Springer, C. Pritchard, Kinase-dead BRAF and oncogenic RAS cooperate to drive tumor progression through CRAF, Cell 140 (2) (2010) 209–221.
[32] H. Shi, G. Moriceau, X. Kong, M.-K. Lee, H. Lee, R.C. Koya, C. Ng, T. Chodon, R. A. Scolyer, K.B. Dahlman, Melanoma whole-exome sequencing identifies V600E B-RAF amplification-mediated acquired B-RAF inhibitor resistance, Nat. Commun. 3 (1) (2012) 724.
[33] P.I. Poulikakos, C. Zhang, G. Bollag, K.M. Shokat, N. Rosen, RAF inhibitors transactivate RAF dimers and ERK signalling in cells with wild-type BRAF, Nature 464 (7287) (2010) 427–430.
[34] C.M. Johannessen, J.S. Boehm, S.Y. Kim, S.R. Thomas, L. Wardwell, L.A. Johnson, C.M. Emery, N. Stransky, A.P. Cogdill, J. Barretina, COT drives resistance to RAF inhibition through MAP kinase pathway reactivation, Nature 468 (7326) (2010) 968–972.
[35] R. Nazarian, H. Shi, Q. Wang, X. Kong, R.C. Koya, H. Lee, Z. Chen, M.-K. Lee, N. Attar, H. Sazegar, Melanomas acquire resistance to B-RAF (V600E) inhibition by RTK or N-RAS upregulation, Nature 468 (7326) (2010) 973–977.
[36] R.B. Corcoran, H. Ebi, A.B. Turke, E.M. Coffee, M. Nishino, A.P. Cogdill, R. D. Brown, P. Della Pelle, D. Dias-Santagata, K.E. Hung, EGFR-mediated reactivation of MAPK signaling contributes to insensitivity of BRAF-mutant colorectal cancers to RAF inhibition with vemurafenib, Cancer Discov. 2 (3) (2012) 227–235.
[37] A. Prahallad, C. Sun, S. Huang, F. Di Nicolantonio, R. Salazar, D. Zecchin, R. L. Beijersbergen, A. Bardelli, R. Bernards, Unresponsiveness of colon cancer to BRAF (V600E) inhibition through feedback activation of EGFR, Nature 483 (7387) (2012) 100–103.
[38] R. Straussman, T. Morikawa, K. Shee, M. Barzily-Rokni, Z.R. Qian, J. Du, A. Davis, M.M. Mongare, J. Gould, D.T. Frederick, Tumour micro-environment elicits innate resistance to RAF inhibitors through HGF secretion, Nature 487 (7408) (2012) 500–504.
[39] R. Antony, C.M. Emery, A.M. Sawyer, L.A. Garraway, C-RAF mutations confer resistance to RAF inhibitors, Cancer Res. 73 (15) (2013) 4840–4851.
[40] H. Cheng, Y. Chang, L. Zhang, J. Luo, Z. Tu, X. Lu, Q. Zhang, J. Lu, X. Ren, K. Ding, Identification and optimization of new dual inhibitors of B-Raf and epidermal growth factor receptor kinases for overcoming resistance against vemurafenib, J. Med. Chem. 57 (6) (2014) 2692–2703.
[41] Z. Eroglu, A. Ribas, Combination therapy with BRAF and MEK inhibitors for melanoma: latest evidence and place in therapy, Therapeutic Advances in Medical Oncology 8 (1) (2016) 48–56.
[42] V. Subbiah, C. Baik, J.M. Kirkwood, Clinical development of BRAF plus MEK inhibitor combinations, Trends in Cancer 6 (9) (2020) 797–810.
[43] O. Hamid, C.L. Cowey, M. Offner, M. Faries, R.D. Carvajal, Efficacy, safety, and tolerability of approved combination BRAF and MEK inhibitor regimens for BRAF-mutant melanoma, Cancers 11 (11) (2019) 1642.
[44] P. Koelblinger, J. Dornbierer, R. Dummer, A review of binimetinib for the treatment of mutant cutaneous melanoma, Future Oncol. 13 (20) (2017) 1755–1766.
[45] S.J. Welsh, P.G. Corrie, Management of BRAF and MEK inhibitor toxicities in patients with metastatic melanoma, Therapeutic Advances in Medical Oncology 7 (2) (2015) 122–136.
[46] C. Glen, Y.Y. Tan, A. Waterston, T.R.J. Evans, R.J. Jones, M.C. Petrie, N.N. Lang, Mechanistic and clinical overview cardiovascular toxicity of BRAF and MEK inhibitors: JACC: CardioOncology state-of-the-art review, Cardio Oncology 4 (1) (2022) 1–18.
[47] C. Scatena, S. Franceschi, M. Franzini, C. Sanguinetti, N. Romiti, L. Caponi, M. Mandalà, C.M. Mazzanti, A.G. Naccarato, Dabrafenib and Trametinib prolong coagulation through the inhibition of tissue factor in BRAF v600e mutated melanoma cells in vitro, Cancer Cell Int. 19 (2019) 1–8.
[48] T. Loyson, E. Werbrouck, K. Punie, L. Bonne, V. Vandecaveye, O. Bechter, Hemorrhage of liver and bone metastases as a result of rapid response to dual BRAF/MEK inhibition in metastatic melanoma: a case report, Melanoma Res. 28 (2) (2018) 147–150.
[49] N.S. Samanci, E. Çelik, O. Bagcilar, B.C. Erol, E. Bicki, K. Oruc, S. Bedir, E. Degerli, S. Derin, N.S. Demirci, Loss of skeletal muscle area and fat-free mass during dabrafenib/trametinib and vemurafenib/cobimetinib treatments in patients with

BRAF-mutant metastatic malignant melanoma, Melanoma Res. 30 (5) (2020) 477–483.
[50] E. Bronte, G. Bronte, G. Novo, G. Rinaldi, F. Bronte, F. Passiglia, A. Russo, Cardiotoxicity mechanisms of the combination of BRAF-inhibitors and MEK-inhibitors, Pharmacol. Ther. 192 (2018) 65–73.
[51] R.I. Mincu, A.A. Mahabadi, L. Michel, S.M. Mrotzek, D. Schadendorf, T. Rassaf, M. Totzeck, Cardiovascular adverse events associated with BRAF and MEK inhibitors: a systematic review and meta-analysis, JAMA Netw. Open 2 (8) (2019) e198890.
[52] M. Liu, X. Yang, J. Liu, B. Zhao, W. Cai, Y. Li, D. Hu, Efficacy and safety of BRAF inhibition alone versus combined BRAF and MEK inhibition in melanoma: a meta-analysis of randomized controlled trials, Oncotarget 8 (19) (2017) 32258.
[53] M.S. Abdel-Maksoud, M.I. El-Gamal, B.S. Lee, M.M. Gamal El-Din, H.R. Jeon, D. Kwon, U.M. Ammar, K.I. Mersal, E.M. Ali, K.-T. Lee, Discovery of new imidazo [2, 1-b] thiazole derivatives as potent pan-raf inhibitors with promising in vitro and in vivo anti-melanoma activity, J. Med. Chem. 64 (10) (2021) 6877–6901.
[54] M.S. Abdel-Maksoud, M.-R. Kim, M.I. El-Gamal, M.M.G. El-Din, J. Tae, H.S. Choi, K.-T. Lee, K.H. Yoo, C.-H. Oh, Design, synthesis, in vitro antiproliferative evaluation, and kinase inhibitory effects of a new series of imidazo [2, 1-b] thiazole derivatives, Eur. J. Med. Chem. 95 (2015) 453–463.
[55] T. Mosmann, Rapid colorimetric assay for cellular growth and survival: application to proliferation and cytotoxicity assays, J. Immunol. Methods 65 (1–2) (1983) 55–63.
[56] L. Vidarsdottir, A. Azimi, I. Das, I. Sigvaldadottir, A. Suryo Rahmanto, A. Petri, S. Kauppinen, C. Ingvar, G. Jönsson, H. Olsson, PTENP1-AS contributes to BRAF inhibitor resistance and is associated with adverse clinical outcome in stage III melanoma, Sci. Rep. 11 (1) (2021), 11023.
[57] M. Hahn, Receptor surface models. 1. Definition and construction, J. Med. Chem. 38 (12) (1995) 2080–2090.
[58] L. Di, E.H. Kerns, Drug-like Properties: Concepts, Structure Design, and Methods, Elevier, London, UK, 2016.
[59] L. Di, E.H. Kerns, N. Gao, S.Q. Li, Y. Huang, J.L. Bourassa, D.M. Huryn, Experimental design on single-time-point high-throughput microsomal stability assay, J. Pharm. Sci. 93 (6) (2004) 1537–1544.
[60] M.J. Kim, H. Kim, I.J. Cha, J.S. Park, J.H. Shon, K.H. Liu, J.G. Shin, High-throughput screening of inhibitory potential of nine cytochrome P450 enzymes in vitro using liquid chromatography/tandem mass spectrometry, Rapid Communications in Mass Spectrometry 19 (18) (2005) 2651–2658.
[61] S.M. Huang, R. Temple, D.C. Throckmorton, L.J. Lesko, Drug interaction studies: study design, data analysis, and implications for dosing and labeling, Clin. Pharmacol. Ther. (St. Louis, MO, U. S.) 81 (2) (2007) 298–304.
[62] M.M. Gamal El-Din, M.I. El-Gamal, M.S. Abdel-Maksoud, K.H. Yoo, D. Baek, J. Choi, H. Lee, C.-H. Oh, Design, synthesis, and in vitro antiproliferative and kinase inhibitory effects of pyrimidinylpyrazole derivatives terminating with arylsulfonamido or cyclic sulfamide substituents, J. Enzyme Inhib. Med. Chem. 31 (sup2) (2016) 111–122.
[63] R. Ramsdale, R.N. Jorissen, F.Z. Li, S. Al-Obaidi, T. Ward, K.E. Sheppard, P. E. Bukczynska, R.J. Young, S.E. Boyle, M. Shackleton, The transcription cofactor c-JUN mediates phenotype switching and BRAF inhibitor resistance in melanoma, Sci. Signal. 8 (390) (2015) ra82-ra82.
[64] M. Fallahi-Sichani, N.J. Moerke, M. Niepel, T. Zhang, N.S. Gray, P.K. Sorger, Systematic analysis of BRAFV 600E melanomas reveals a role for JNK/c-Jun pathway in adaptive resistance to drug-induced apoptosis, Mol. Syst. Biol. 11 (3) (2015) 797.
[65] T. Danker, C. Möller, Early identification of hERG liability in drug discovery programs by automated patch clamp, Front. Pharmacol. 5 (2014) 87849.